

https://dspace.org/

Promotion effects of iron in carbon nanotubes synthesis to make supports for Fischer-Tropsch synthesis catalysts

Kente, Thobeka

2011-03-11
http://hdl.handle.net/10539/9147

Downloaded from a DSpace repository. https://dspace.org/

Promotion effects of iron in carbon nanotubes synthesis to make supports for Fischer-Tropsch synthesis catalysts.

BY

Thobeka Kente

A dissertation submitted to the Faculty of Science, University of the Witwatersrand, Johannesburg, in fulfillment of the requirements for the Masters degree.

SEPTEMBER 2010

Declaration

I declare that this dissertation is my own original work. It has not been submitted before for the Degree of Masters of Science in the University of the Witwatersrand, Johannesburg. It has not been submitted before for any degree or examination in any other University.

Signature of candidate ……..

On this……day of……2010

Dedication

I dedicate this to the following people:

- *To the memory of my mom, who was encouragement when I was discouraged, who was wise when I was stupid, who cared when I was careless. thank you so much for educating me , making me the person I am today.*

- *To my sisters, brothers, nieces, nephews.*

- *All of my friends.*

I thank all of you for being part of my life.

Acknowledgement

I would like to thank the following people:

- God for giving me strength to write up all of this.
- My supervisor Professor N.J Coville for the guidance, giving advices, encouraging and supporting in this project.
- Basil for the technical assistance.
- Professor Michael Witcomb, Caroline and Abe for their help in electron microscope unit.
- My family for believing in me, and giving the moral support.
- My colleagues CATOMAT group for friendly environment I enjoyed to work with you guyz
- NRF grant holder for financial assistance
- KEM for prayers
- Dr Sabelo Mhlanga, for reading this dissertation.

Abstract

Iron (Fe), catalysts were prepared by incipient wetness impregnation method using $CaCO_3$ as a supporter. 0.6% Cu, 0.4% K, 0.6% Cu/0.4% K, 0.1 ml of Tetraethyl orthosilane (TEOS) in 2ml water were used as promoters for the Fe catalysts. The promoted catalysts were then employed in the synthesis of carbon nanotubes (CNTs) using a chemical vapor deposition (CVD) method. Transmission electron microscopy (TEM) revealed that Cu increased the diameter of the CNTs and caused them to be coiled, thereby altering the shape of the CNTs. The addition of K resulted in no recognizable change in the microstructure of these tubes. The CNTs obtained looked similar to those obtained when Fe was used without a promoter. However, the diameter of the tubes also increased due to K addition.

Thermol Gravimetric Analysis (TGA) results showed that the addition of K to the Fe catalyst (Figure 20, p56, 57) resulted in the enhancement in thermal stability of the CNTs. BET analysis revealed that Cu increased the surface area while K decreased the surface area of this solid material. The Cu/K promoted catalyst produced CNTs with diameters of 60 nm which was the same as unpromoted catalyst. However, the CNT diameter distribution was quiet different for the two catalysts. The surface area was less than that of the unpromoted catalyst. The Fe/Cu/K synthesized CNTs were coiled and they looked more like the product produced from Fe/Cu CNTs. Thus the Cu catalyst has the dominant effect in determining the CNT morphology. When SiO_2 was used as a promoter no change in the diameter distribution of the CNTs could be detected. Thus while changes to the carbon surface may have occurred at the atomic level, the changes were not detected at the TEM resolution used. The surface area was also less than that of CNTs produced over the unpromoted catalyst.

Both promoted and unpromoted Fe/CNT were tested for FT synthesis. The activity, selectivity and CO conversions were recorded. The K was found to strongly influence the production of the hydrocarbon yield and increased the CO conversion. The K promoted catalyst increased the CO reaction rate, and increased the olefinity and the alpha value. The effect of K on the olefinity of the C_2 hydrocarbon ranged from 0.04 to 0.26. An increase in FTS activity is also observed for the K promoted catalyst. Cu decreased the reduction temperature of Fe oxides as noted by TPR

studies. The Cu promoted catalyst showed a high selectivity to methane and a decrease of C_{5+} hydrocarbons, the C_2 olefins also decreased.

Poster and Oral presentations arising from this dissertation

- South African Nanotechnology Initiative (SANI) conference 2009, CSIR convention centre, Pretoria: Poster presentation
- Cross faculty postgraduate symposium at Wits 2009: Poster presentation
  The effect of promoters (Cu,K) on the synthesis of iron catalysts supported on carbon nanotubes .
- Center of Excellence in Strong Materials Seminar, Humphrey Raikes Building 2009, Wits University: Oral presantation.
  Effect of promoters (Cu, K and Cu/K) on the synthesis of iron catalysts supported on carbon nanotubes
- CATOMAT group seminar, Humphrey raikes Building 2009, Wits Univerity: Oral presantation.
  Effect of promoters (Cu, K and Cu/K) on the synthesis of iron catalysts supported on carbon nanotubes

Table of Contents

List of Tables. xi

List of Figures. xii

Nomenclature. xv

Chapter 1 1

Introduction 1

1.1 Carbon nanotubes 1

1.1.1 History & Development 1

1.1.2 Multiwalled Carbon Nanotubes 3

1.1.3 Singlewalled Carbon Nanotubes 4

1.2 Properties and applications of carbon nanotubes 4

1.2.1 Field Emission 5

1.2.2. Conductive Plastics 5

1.2.3. Energy Storage 6

1.2.4. Conductive Adhesives and Connectors 6

1.2.5. Molecular Electronics 6

1.2.6. Thermal Materials 7

1.2.7. Structural Composites 7

1.2.8. Fibres and Fabrics 7

1.2.9. Catalyst Supports 7

1.2.10. Biomedical Applications 8

1.2.11 Other Applications 8

1.3 Synthesis of carbon nanotubes 8

1.3.1. Arc discharge 9

1.3.2. Laser ablation 10

1.3.3. Chemical vapour method (CVD) 10

1.4 Growth mechanism 10

1.5 Characterisation of carbon nanotubes 11

1.5.1 Electron microscopy (EM) 12

1.5.2 Raman spectroscopy 13

1.5.3 Brunuer-Emmett and Teller (BET) 13

1.6 The Fisher-Tropsch Synthesis 14

1.6.1 History and development 14

1.6.2 Process reactors 15

1.6.3. Fisher-Tropsch catalysts 16

1.6.4. Promoter effects 17

1.7 Aims and objectives of this study 18

1.8 References 22

Chapter 2 28

Experimental methods 28

2.1 Carbon nanotubes. 28

2.1.1 Preparation of catalysts 28

2.1.2 Synthesis of CNTs 29

2.1.3 Purification of carbon nanotubes 30

2.2 Fischer-Tropsch 31

2.2.1 Synthesis of catalysts supported on CNTs 31

2.2.2 Preparation of Catalysts. 31

2.2.3 Fisher-Tropsch synthesis 31

2.3 Characterisation techniques 35

2.3.1 N_2 Physisorption 35

2.3.2 Transmission electron microscopy (TEM) 35

2.3.3 Thermogravimetric analysis (TGA) 35

2.3.4 Raman Spectroscopy 35

2.3.5 Scanning electron microscopy (SEM) 36

2.3.6 Energy dispersive X-ray (EDX) 36

2.3.7 Temperature programmed reduction (TPR) 36

2.3.8 Inductive Coupled Plasma-Optical Emission Spectroscopy (ICP-OES) 37

2.4 References 38

Chapter 3 39

Results and Discussion 39

3.1 Introduction 39

3.1.1 Effect of copper (Cu) on carbon nanotube production 41

3.1.2 Effect of potassium (K) on carbon nanotube production 47

3.1.3 Effect of co-addition of copper and potassium to Fe/$CaCO_3$ 51

3.1.4 Effect of SiO_2 on carbon nanotubes production. 56

3.1.5 Thermogravimetric Analysis (TGA) of CNTs performed in air 61

3.1.6 Effect of temperature and promoter loading on the Fe catalyst. 64

3.1.7 Effect of carrier gas on CNT production 67

3.2 Conclusion 71

3.3 References 72

Chapter 4 74

Results and Discussion 74

4.1 Introduction 74

4.1.1 Catalyst characterization for FT synthesis 76

4.1.2. Reduction behavior of the catalysts 78

4.1.3 Catalyst test, data analysis and calculations 80

4.1.4 Catalytic performance 81

4.1.5 Product selectivity 83

4.2 Conclusions 87

4.3 References 88

Chapter 5 90

5.1 General conclusions 90

5.2 Future Research 91

List of Tables.

Table 1.1: Features of different techniques for the synthesis of carbon nanotubes

Table 3.1: Peak positions and the intensity ratio data (I_D/I_G) for the purified samples (a) Fe (b) Fe- Cu

Table 3.2: Peak positions and intensity ratios for the purified samples (a) Fe (b) Fe-K .

Table 3.3: Peak positions of the purified samples (a) Fe (b) Fe-Cu-K and the intensity ratio of the bands.

Table 3.4: Peak positions of the purified samples and the intensity ratio of the bands

Table 3.5: Data from the derivative curves.

Table 3.6: Properties of purified MWCNTs produced as a function of promoter loading

Table 3.7: Comparison of data for the synthesis of CNTS produced from this study and similar literature studies.

Table 3.8: Reaction conditions of the synthesis of CNTs under H_2

Table 3.9: Reaction conditions of the synthesis of CNTs under N_2

Table 4.1: Different levels of promoters and supports

Table 4.2: Metal content of various catalysts determined by ICPOES

Table 4.3: Surface area analysis of catalyst determined by BET

Table 4.4: Fe peak positions of the catalyst obtained from a TPR profile.

Table 4.5: Activity, CO conversion and Selectivity of iron catalyst.

Table 4.6: Product selectivity of the catalysts

List of Figures.

Figure 1.1: Various forms of carbon

Figure 1.2: TEM images of (a) MWCNTs (b) SWCNTs and a graphical representation of the formation of SWCNTs (c) and (d) MWCNTs

Figure 1.3: Visualisation of a possible carbon nanotube growth mechanism

Figure 1.4: Fluidised bed FT reactors: (A) CFB reactor; (B) ebulating or FFB reactor; (C) Slurry phase bubbling bed reactor

Figure 2.1: CVD setup used for the synthesis of CNTs

Figure 2.2: F-T reactor with temperature controller, FID, TCD and Computer.

Figure 3.1: TEM and SEM images of the product produced from (a) Fe (b) Fe-Cu catalysts at 600ºC for 1 hour

Figurer 3.2: Diameter distribution of the products produced from (a) Fe (b) Fe-Cu catalyst at 600ºC Figure 3: EDX spectrum of purified Fe-Cu CNTs

Figure 3.4: Surface area of (a) Fe (b) Fe-Cu CNTs

Figure 3.5: Raman spectra of (a) 10% Fe (b) 10%Fe-0.6%Cu materials

Figure 3.6: TEM and SEM images of the product produced from Fe and Fe-K catalyst at 600ºC

Figure 3.7: Diameter distribution of the product produced from (a) Fe (b) Fe-K catalysts at 600ºC

Figure 3.8: EDX spectrum of purified Fe-K CNTs

Figure 3.9: Surface area of (a) Fe (b) Fe-K CNTs

Figure 3.10: Raman spectra of (a) 10% Fe (b) 10%Fe-0.4%K materials

Figure 3.11: TEM images of the product produced from (a) Fe (b) Fe-K-Cu catalyst at 600ºC

Figurer 3.12: Diameter distribution of the products produced from the (a) Fe (b) Fe-Cu-K catalysts at 600ºC

Figure 3.13: Surface area of (a) Fe (b) Fe-K-Cu CNTs

Figure 3.14: Raman spectra of (a) 10% Fe (b) 10%Fe-0.6%Cu/0.4%K material

Figure 3.15: TEM and SEM images of the product produced from Fe and Fe-SiO_2 catalyst at 600ºC

Figure 3.16: Diameter distribution of the product produced from (a) Fe-SiO_2 (a) Fe catalyst at 600ºC

Figure 3.17: EDX spectrum of purified Fe-SiO_2 CNTs

Figure 3.18: Surface area of (a) Fe (b) Fe-SiO_2 CNTs

Figure 3.19: Raman spectra of (a) 10% Fe (b) 10%Fe-0.1%SiO_2 samples

Figure 3.20: TGA (a) Fe, Fe/Cu, Fe/K, Fe/Cu/K, Fe/SiO_2 profiles and (b) Fe, Fe/Cu, Fe/K, Fe/Cu/K, Fe/SiO_2 derivative curves of purified CNTs.

Figure 3.21 : Yield of Fe, Fe-K, Fe-Cu obtained over temperature 600, 650 and 700ºC

Figure 3.22 : Yield obtained over 10%Fe, 10%Fe-0.4%Cu and K, 10%Fe-0.6%Cu and K, 10%Fe-1%Cu and K catalyst containing various amount of loadings of Cu an K promoters.

Figure 3. 23: TEM images of unpurified CNTs (a) 10%Fe (N_2) (b) 10%Fe (H_2)

Figure 3.24: TEM and SEM images of unpurified CNTs (a) 10%Fe (b) Fe-0.6%Cu (c) Fe-0.2%K at 700ºC under N_2

Figure 3.25: TGA profile of (a) unpurified and (b) purified CNTs

Figure 4.1: Chain growth and termination

Figure 4.2: TEM image of 10%Fe/CNTs, 10%Fe-0.6%Cu/CNTs, and 10% Fe-0.4% K.

Figure 4.3: TPR profiles of 10%Fe/CNTs, 10%Fe-0.6%Cu/CNTs, 10%Fe-0.4%K.

Figure 4.4: CO conversions with time on stream of (a) Fe/CNT (b) Fe-Cu/CNT (c) Fe-K/CNT.

Figure 4.5 Anderson–Schulz–Flory (ASF) Carbon number distribution of hydrocarbons formed over unpromoted Fe and Cu, K promoted iron catalyst.

Nomenclature.

Al_2O_3	Aluminium oxide
ASF	Anderson-Schulz-Flory
BET	Brunauer-Emmett-Teller
C %	Carbon deposit percentage
C_2H_2	Acetylene
C_2H_4	Ethylene
$CaCO_3$	Calcium carbonate
CaO	Calcium oxide
CCVD	Catalytic chemical vapour deposition
CNT(s)	Carbon nanotube(s)
CO_2	Carbon dioxide
CFB	Circulating fluidized bed reactor
CS(s)	Carbon sphere(s)
$Cu(NO_3)_3.9H_2O$	Copper nitrate
CVD	Chemical vapour deposition
DWCNT(s)	Double walled carbon nanotube(s)
EDX	Energy dispersive X-ray spectroscopy
EM	Electron micscopy
Fe	Iron
$Fe(NO_3)_3.9H_2O$	Iron nitrate
FFB	Fixed fluidized bed
FID	Flame ionization detector
FT	Fischer-Tropsch
FTS	Fischer-Tropsch synthesis
H	Hour
H_2	Hydrogen
HF	Hydrofluoric acid
HNO_3	Nitric acid
HTFT	High temperature Fischer Tropsch

ICP-AES	Inductively coupled plasma-atomic emission spectroscopy
KNO_3	Potassium nitrate
LTFT	Low temperature Fischer Tropsch
ml/min	Millilitre per minute
MWCNT(s)	Multi walled carbon nanotubes(s)
N_2	Nitrogen
nm	Nanometre
SEM	Scanning electron microscopy
SiO_2	Silicon dioxide
SWCNT(s)	Single walled carbon nanotubes(s)
t	Time
T	Temperature
TCD	Thermal conductivity detector
TFBR	Tubular fixed bed reactor
TEM	Transmission electron microscopy
TEOS	Tetraethoxyorthosilane
TGA	Thermogravimetric analysis
TPR	Temperature–Programmed –Reduction
WGS	Water gas shift
wt%	Weight percentage.
α	Alpha value

Chapter 1

Introduction

1.1 Carbon nanotubes

This section gives a short overview on carbon nanotubes (CNTs). This includes a brief overview of the history and development, applications and properties, synthesis, growth mechanism, and characterization of CNTs. A review of the application of CNTs as catalyst support in Fischer-Tropsch synthesis is presented.

1.1.1 History & Development

CNTs were reported by Iijima in 1991[1]. Ijima initially observed only multi walled carbon nanotubes (MWCNTs) between 2 and 20 layers. Later in 1993 he reported the discovery of single walled carbon nanotubes (SWCNTs) and revealed their structure. The discovery of CNTs is linked to the discovery of the Buckyball by scientists in the late 1980's. In a Radioastronomy study, scientists established unusually long molecules that had not been synthesised in a laboratory. Their concentration was much higher than everyone expected. The synthesis of these long carbon chains was attempted in the laboratory by scientists. They used a powerful laser to evaporate small amounts of graphite into a hot cloud of particles, and then cooled the cloud with a stream of helium gas [2]. In this way buckyballs were synthesized.

Buckyballs are made up of 60 carbon atoms (C_{60}), ordered in the shape of a sphere (Figure 1). In fact, what had been discovered was not just a single new molecule but an infinite class of new molecules: the fullerenes. Each fullerene (C_{60}, C_{70}, C_{84}, etc.) possessed the essential characteristic of being a pure carbon cage, each carbon atom being bonded to three others as observed in graphite. Unlike graphite the fullerenes are not planar due to the presence of pentagons. Every fullerene has exactly 12 pentagonal faces with a varying number of hexagonal faces (e.g., buckyball – C_{60} – has 20 hexagonal faces).

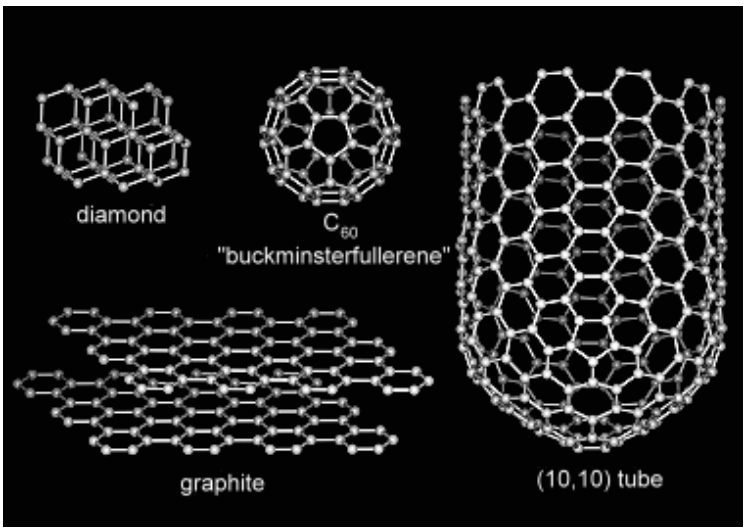


Figure 1.1: Various forms of carbon [2].

Some fullerenes, like C_{60}, are spheroidal in shape, and others, like C_{70}, have a rhombus shape like a rugby ball. Smalley et al [1] discovered in 1990 that, in principle, a tubular fullerene should be possible, capped at each end, for example, by the two hemispheres of C_{60}, connected by a straight segment of tube, with only hexagonal units in its structure. Dresselhaus et al, dubbed these imagined objects "buckytubes." [3].

A nanotube may consist of one tube of graphite (SWCNT), or a number of concentric tubes giving rise to so called (MWCNTs) (Figure 2(c) and (d)).When viewed under a transmission electron microscope (TEM) SWCNTs appear as two planes, MWCNTs more than two graphite sheets are observed, and can be seen as parallel lines [4] (Figure 2 (a) and (b)). The SWCNTs are generally narrower than the MWCNTs, with diameters typically in the range of 1-2 nm [5], and they tend to be curved rather than straight.

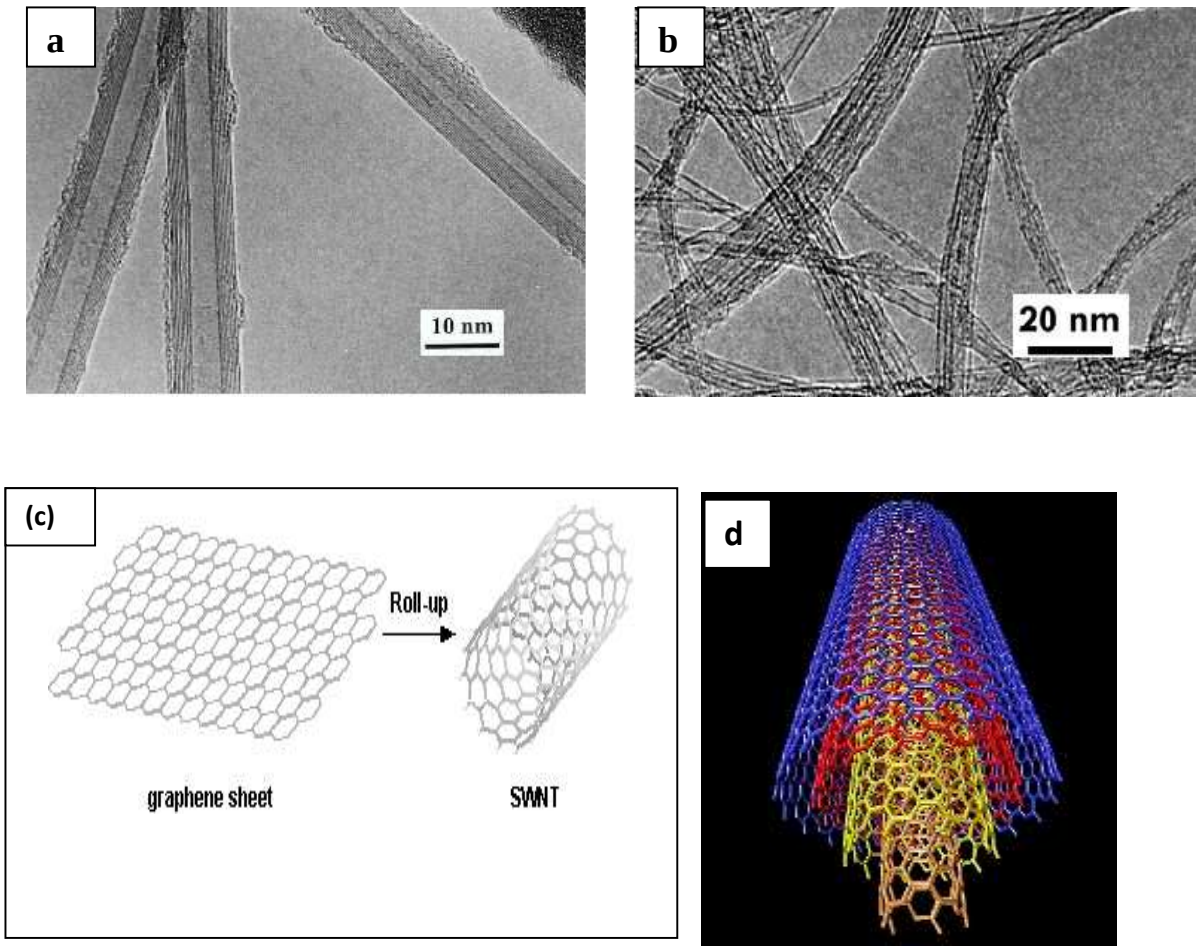


Figure 1.2: TEM images of (a) MWCNTs (b) SWCNTs and a graphical representation of the formation of SWCNTs (c) and (d) MWCNTs [5, 6]

1.1.2 Multiwalled Carbon Nanotubes

Ten years after Iijima's initial observation, much has been said about nanotubes and tubular fullerenes. MWCNTs are generally produced with a high frequency of structural defects. In comparison with their larger relations, the 5-20 micron-diameter graphite fibers, MWCNTs are quite sound structurally; nevertheless, they frequently contain regions of structural imperfection. The occurrence of defects leads to inevitable degradation of the material properties of the substance, such as strength. Typically the actual properties of a bulk material are only a few percent of what the material would exhibit if it were structurally perfect. For example, a structural defect such as a microcrack in a steel wire, will lead to catastrophic failure at 1-2% of

the theoretical breaking strength that would be predicted based on fundamental chemical principals [3].

1.1.3 Singlewalled Carbon Nanotubes

SWCNTs are a very important variant of CNTs. They exhibit important electrical properties that are not observed in the MWCNTs. SWCNTs can be used for miniaturizing electronics beyond the micro electromechemical scale that is currently the basis of modern electronics. The most basic building block of these systems is the electric wire, and SWNTs, because they are excellent conductors may eventually be useful in the electronic world [7].

1.2 Properties and applications of carbon nanotubes

The major properties of CNTs are the optical properties. Thermal properties of CNTs have great implications for science and CNTs are said to also have elastic properties as well [8]. Preliminary experiments and simulation studies on the thermal properties of CNTs show that they have very high thermal conductivity. It is expected, therefore that nanotube reinforcements in polymeric materials may also significantly improve the thermal and thermomechanical properties of the composites [9].

CNTs have attracted considerable attention because of their potential applications in nanoelectronics [10-13], energy storage [14-16], as catalyst supports [17] and in many other devices [18-21].They have extraordinary electrical conductivity, heat conductivity and mechanical properties. Others have reported that the CNTs could be the best electron field-emitters possible. Ideally they are polymers of pure carbon and can be reacted and manipulated using the tremendously rich chemistry of carbon. This provides an opportunity to modify the structure and to optimise their solubility and dispersion. Very significantly; CNTs are in principle molecularly perfect, which means that they are free of property-degrading flaws in the nanotube structure [22]. These extraordinary characteristics give CNTs potential in various applications. Some examples of CNT applications are described below.

1.2.1 Field Emission

CNTs are the best known field emitters of any material. This is understandable, given their high electrical conductivity, and the sharpness of their tip (the sharper the tip, the more concentrated will be an electric field, leading to field emission; this is the same reason lightening rods are sharp). The sharpness of the tip also means that they emit at especially low voltage, an important aspect for building electrical devices that utilize this feature. CNTs can carry a very high current density, possibly as high as 1013 A/cm^2. Furthermore, the current is extremely stable [23]. The high current density, low turn-on and operating voltage, and steady, long-lived behaviour make CNTs attractive field emitters to enable this application. Other applications utilising the field-emission characteristics of CNTs include: general cold-cathode lighting sources, lightning arrestors, and electron microscope sources.

1.1.2. Conductive Plastics

Much of the history of plastics over the last half century involves using the plastics as a replacement for metals. For structural applications, plastics have made a tremendous headway. However, when electrical conductivity is required, plastics are unsuitable since they are good electrical insulators. This deficiency is overcome by loading plastics with conductive fillers, such as carbon black and graphite fibres (e.g to make golf clubs and tennis racquets). The loading required to provide the necessary conductivity is typically high, and results in heavy parts. More importantly the structural properties are highly degraded by plastic parts.

It is well established that the higher the aspect ratio of the filler, the lower the loading required to achieve a given level of conductivity. CNTs are ideal in this sense, since they have the highest aspect ratio of any carbon fibre. In addition, their natural tendency to form ropes provides essentially very long conductive pathways even at ultra-low loadings [22].

1.2.3. Energy Storage

CNTs have the essential characteristics desired in materials used as electrodes in batteries and capacitors, two technologies of rapidly increasing importance. CNTs can have a tremendously high surface area (~1000 m^2/g), good electrical conductivity, and more importantly, their linear geometry makes their surfaces highly accessible to an electrolyte.

Research has shown that CNTs have the highest reversible capacity of any carbon material for use in lithium-ion batteries [24]. In addition, CNTs are outstanding materials for supercapacitor electrodes [25] and are now being marketed.

CNTs also have applications in a variety of fuel cell components. They have a number of properties including high surface area and thermal conductivity that make them useful as electrode catalyst supports in proton exchange membrane (PEM) fuel cells. They may also be used in gas diffusion layers as well as in current collectors because of their high electrical conductivity. The high strength and toughness to weight characteristics of CNTs may also prove valuable when used as composite components in fuel cells that are deployed in transport applications where durability is extremely important [22].

1.2.4. Conductive Adhesives and Connectors

The same properties that make CNTs attractive as conductive fillers for use in shielding etc; makes them attractive for use in other important materials, such as adhesives and other connectors such as solders.

1.2.5. Molecular Electronics

The idea of building electronic circuits out of the essential building blocks of materials - molecules has seen a revival. Electronic circuitry is a key component of nanotechnology. In any electronic circuit, but particularly as dimensions shrink to the nanoscale, the interconnections between switches and other active devices become increasingly important. Their geometry, electrical conductivity, and ability to be precisely derived, make CNTs the ideal candidates for

the connections in molecular electronics. In addition, they have been demonstrated as switches themselves [22].

1.2.6. Thermal Materials

The record-setting anisotropic thermal conductivity of buckytubes is enabling applications where heat needs to move from one place to another. Such an application in electronics, particularly advanced computing, using uncooled chips is now routinely possible where temperatures can reach over 100^{o}C. Chickasaw Nation Industries (CNI) technology for creating aligned structures and ribbons of CNTs [26] is a step toward realising efficient heat conduits. In addition, composites with CNTs have been shown to dramatically increase bulk thermal conductivity at small loadings.

1.2.7. Structural Composites

The world-record properties of CNTs are not limited to electrical and thermal conductivities, but also include mechanical properties, such as stiffness, toughness and strength. These properties lead to a wealth of applications, including advanced composites requiring high values in one or more of these properties [27].

1.2.8. Fibres and Fabrics

Fibres spun of pure CNTs have recently been demonstrated [9] and are undergoing rapid development, along with buckytube composite fibres. Such super strong fibres will have applications including body and vehicle armour, transmission line cables, woven fabrics and textiles.

1.2.9. Catalyst Supports

Open CNTs have an essentially high surface area; in fact, every atom is not just on a surface - each atom is on two surfaces, the inside and outside! Combined with the ability to attach

essentially any chemical species to their sidewalls, this provides an opportunity for unique catalyst supports. Their electrical conductivity may also be exploited in the search for new catalysts and catalytic behaviour [29].

1.2.10. Biomedical Applications

The exploration of CNTs in biomedical applications is underway, and has significant potential. Cells have been shown to grow on CNTs, so they appear to have no toxic effect. The cells also do not adhere to the CNTs; potentially giving rise to applications such as coatings for prosthetics and anti-fouling coatings for ships. The ability to chemically modify the sidewalls of CNTs also leads to biomedical applications such as in vascular stents, and for neuron growth and regeneration. [29]

1.2.11 Other Applications

There is a wealth of other potential applications for CNTs, such as solar collection; nanoporous filters; and coatings of all sorts. There are almost certainly many unanticipated applications for this remarkable material that will come to light in the years ahead and which may prove to be important and valuable.

1.3 Synthesis of carbon nanotubes

There has been intensive research into the production of CNTs in recent years as they are novel nanomaterials with unique properties that promise advances in a diverse number of areas with many potential applications. Various CNT preparation methods have been reported and these methods include arc-discharge [30-32], laser ablation [33-35] and chemical vapor deposition (CVD) [36-38]. Among these methods, catalytic chemical vapor deposition appears to be the most promising way for producing MWCNTs in large scale with good quality at a relatively low cost [39].

Table 1 presents some typical characteristics for each technique in terms of yield of (SWCNTs) or (MWCNTs) and the carbon nanotube diameter. [40]

Table 1.1: Features of different techniques for the synthesis of carbon nanotubes [40]

	Arc Discharge	Laser Ablation	CVD
Yield	30-90%	<70%	20-100%
Diameter of SWCNT	0.6-1.4 nm	1-2 nm	0.6-4 nm
Diameter of MWCNT	1-3 nm	-	12-240 nm

The CVD method requires the use of both a catalyst (typically Fe, Co or Ni) and a carbon source to produce MWCNTs or other novel carbon 'shaped' materials. The two typical CVD methodologies require either a floating catalyst [41-43] or a solid catalyst typically deposited on a support [44-45].

1.3.1. Arc discharge

The arc discharge technique involves a simple set up and the method can produce CNTs in high yield. This was the method originally used by Iijima [46] for the production of buckyball structures and CNTs. It comprises the vaporization of one of two carbon electron rods, placed end-to-end, with a current passing through the pair. The high temperature of the discharge causes the consumption of one of the rods. The consumed rod (anode) can be found deposited on the end of the other rod (cathode) in the form of soot, occasionally described as a 'cigar-like' structure that contains nanotubes. A 'bowl' shaped cathode used by Huang [47] has the added advantage that it allows for a greater surface area, decreasing the defects in the product and producing cleaner carbon nanotubes. The cathode also acts as a good collector. The rods must be kept at a constant distance apart of approximately 1-2 mm.

1.3.2. Laser ablation

Laser irradiation offers much more space and time control during the interaction process than the former method. However, the composition of the target material also plays an important role in the production of CNTs. It is commonly observed that by evaporation of pure graphite, MWNTs are produced. Graphite doped with small amounts of certain kinds of metals enhances the growth of SWCNTs. Not only is the chemical composition important, but also the target's physical properties, i.e. roughness, porosity and thermal conductivity. These physical properties have an influence on the dissipation of the incoming laser radiation and as a consequence of heat and evaporation, as has been demonstrated by several authors. It is a promising and not so expensive alternative to conventional synthesis routes [34]

1.3.3. Chemical vapour method (CVD)

The (CVD) method is most commonly used for the production of CNTs and it is a chemical process used to produce high-purity, high-performance solid materials. The CVD process is often used in the semiconductor industry to produce thin films. During CVD, a substrate is prepared with a layer of metal catalyst particles most commonly Ni, Co, Fe, or a combination of the metals. The metal nanoparticles can also be produced by other methods e.g. by reduction of oxides or solid oxide solutions. The diameters of the nanotubes that are to be grown are related to the size of the metal particles. In a typical CVD process, the substrate is exposed to one or more volatile precursors, which react and/or decompose on the substrate surface to produce the desired deposit. Frequently, volatile by-products are also produced, which are removed by gas flow through the reaction chamber [48].

1.4 Growth mechanism

The way in which CNTs are formed is not exactly known. The growth mechanism is still a subject of controversy, and more than one mechanism might be operative during the formation of CNTs. In this section, the possible mechanism of supported CVD synthesized CNTs is reported. When weak interactions between the metal and the support exist, then the tip growth mechanism is observed and when strong interactions exist then the extrusion/root/base growth mechanism is observed [49]. The mechanisms are listed in Figure 3. First a precursor to the formation of

nanotubes and fullerenes, C_2, is formed on the surface of the metal catalyst particle. From this a metastable carbide particle, a rodlike carbon, is rapidly formed. Secondly there is a slow graphitization of carbon on the metal wall. This mechanism is based on in-situ TEM observations [50]. The exact atmospheric condition depends on the technique used. The actual growth of the nanotube seems to be the same for all the methods mentioned above.

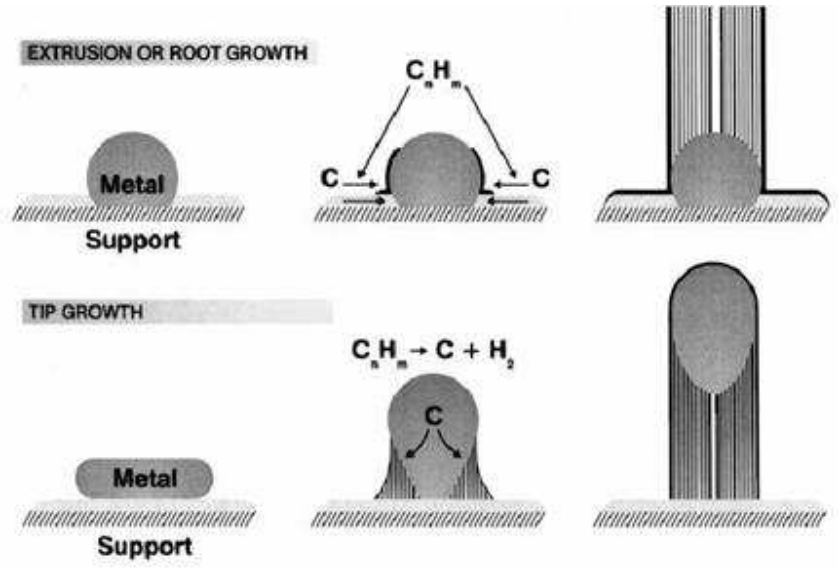


Figure 1.3. Visualisation of a possible carbon nanotube growth mechanisms [49].

1.5 Characterisation of carbon nanotubes

CNTs due to their specific atomic structure have interesting chemical and physical properties different to those of graphite and diamond. These properties can be measured and characterized by a range of techniques. Transmission electron microscopy (TEM), scanning electron microscopy (SEM), thermogravimetric analysis (TGA), Raman spectroscopy, Brunauer, Emmett and Teller (BET) surface area and prosity analysis, and powder X-ray diffraction (PXRD). The most important characterization techniques are discussed below [51].

1.5.1 Electron microscopy (EM)

TEM is a technique used to study the morphology, crystallographic structure, and even composition of a specimen. TEM provides a much higher spatial resolution than SEM and can facilitate the analysis of features at the atomic scale (in the range of a few nanometers) using electron beam energies in the range of 60 to 350 keV.

TEM uses an electron gun to produce the primary beam of electrons that will be focused by lenses and apertures into a very thin, coherent beam. This beam is then controlled to strike the specimen. A portion of this beam gets transmitted to the other side of the specimen, is collected, and processed to form the image.

For crystalline materials, the specimen diffracts the incident electron beam, producing local diffraction intensity variations that can be translated into contrast to form an image. For amorphous materials, contrast is achieved by variations in electron scattering as the electrons traverse the chemical and physical differences within the specimen [52]. The greatest consideration when performing TEM analysis is sample preparation. The quality of sample preparation contributes greatly to whether the micrograph will be good or not.

SEM is used for inspecting topographies of specimens at very high magnifications. SEM magnifications can go to higher than 300,000 X but most semiconductor applications require magnifications of about 3,000 X only. During SEM inspection, a beam of electrons is focused on a spot volume of the specimen, resulting in the transfer of energy to the spot. To produce the SEM image, the electron beam is swept across the area being inspected, producing many such signals. These signals are then amplified, analyzed, and translated into images of the topography being inspected.

The SEM and TEM equipment may be equipped with an Energy dispersive X-ray (EDX) analysis system to enable it to perform compositional analysis on specimens. EDX analysis is useful in identifying elements and contaminants, as well as estimating their relative concentrations on the surface of the specimen [52].

1.5.2 Thermogravimetric analysis (TGA)

TGA is a simple analytical technique that measures the weight loss (or weight gain) of a material as a function of temperature. As materials are heated, they can lose weight from a simple process such as drying, or from chemical reactions that liberate gases. Some materials can gain weight by reacting with the atmosphere in the testing environment. Since weight loss and gain are disruptive processes to the sample material or batch, knowledge of the magnitude and temperature range of those reactions are necessary in order to design adequate thermal ramps and holds during those critical reaction periods [53].

1.5.3 Raman spectroscopy

Raman spectroscopy is one of the most powerful tools for characterization of CNTs. Without sample preparation, a fast and non-destructive analysis is possible. All allotropic forms of carbon are active in Raman spectroscopy [54]: fullerenes, carbon nanotubes, amorphous carbon, polycrystalline carbon, etc. The position, width, and relative intensity of bands are modified according to the carbon forms [55].

1.5.4 Brunauer-Emmett and Teller (BET)

The BET method is the most popular method used to determine total surface area of materials. This method is used to determine the specific surface area, pore volume and pore size distribution of a sample. The determination of surface area is considered to be an important requirement in catalyst characterization, although the catalytic activity may only be indirectly related to the total surface area [56].

1.5.5 Powder X-ray diffraction (PXRD)

Powder X-ray diffraction is a non-destructive technique widely applied for the characterisation of crystalline materials. The method has been traditionally used for phase identification, quantitative analysis and the determination of structure imperfections. The method is normally applied to data collected under ambient conditions, but *in situ* diffraction as a function of

external constraints (temperature, pressure, stress, electric field, atmosphere, etc.) is important for the interpretation of solid state transformations and materials behaviour. Various kinds of micro- and nano-crystalline materials can be characterised from X-ray powder diffraction, patterns including inorganics, organics, drugs, minerals, zeolites, catalysts, metals and ceramics. The physical states of the materials can be loose powders, thin films, polycrystalline and bulk materials. For most applications, the amount of information which is possible depends on the nature of the sample microstructure, the complexity of the crystal structure and the quality of the experimental data [57].

1.6 The Fischer-Tropsch Synthesis.

This section describes an overview of the Fisher-Tropsch (FT) process. The history and development of Fischer-Tropsch synthesis, process reactors, Fischer-Tropsch catalysts and promoter effects all are described below.

1.6.1 History and development

The Fischer-Tropsch (FT) process was discovered by German scientists and used to make fuels during World War II. There has been continued interest of varying intensity in Fischer-Tropsch technology ever since. The FT reaction converts a mixture of hydrogen and carbon monoxide derived from coal, methane, or biomass to liquid fuels [58]. Since the discovery of the FT reaction in the 1920s, the industrial catalysts of choice have proven to be cobalt and iron. Either Co or Fe is typically used in combination with a range of supports and promoters that permit further control over the product selectivity. In particular it has been reported that a mixture of the two most active catalysts, Fe and Co, have generated product streams in the FT reaction richer in olefins and alcohols than expected from either Fe or Co catalysts [59].

Fe is known to be a catalyst that forms carbon/polymers/oligomers including MWCNTs from a range of carbon sources. Fe has also been found to be one of the two industrial metals of choice in the FT reaction. In this reaction $CO + H_2$ are converted to $(CH_2)_x$ ($x>1$) oligomers, typically for use in the chemicals and fuel industry. This suggests that promoters that are known to modify the Fe FT reaction could have applicability in MWCNT synthesis [60]. In industrial applications,

a high performance catalyst plays an essential role. In the FT process, the catalyst activity and selectivity are influenced by the metal dispersion, metal loading, and catalyst preparation methods [61]

1.6.2 Process reactors

There are many reactors that are currently used for the FT reaction. The types of reactors are divided into two categories: The first type of reactor is used for high temperature Fischer-Tropsch (HTFT) synthesis and the second one is used for low temperature Fischer-Tropsch (LTFT) synthesis. The difference between the two is that LTFT is mainly used for the production of wax whereas HTFT is mainly used for the production of alkenes and gasoline [62].

The tubular fixed bed reactor (TFBR) was used for LTFT at Sasol. These reactors had many disadvantages e.g. high pressure drop [63]. Another type of LTFT (Sasol slurry bed reactor) was thus developed and commissioned in 1993 at Sasol and has a number of advantages over the TFBR. It is very easy to control temperature in the reactor due to the well mixed state in the reactor; the pressure drop is very low and the catalyst can be added on line. Low temperature operation of this reactor favours wax production and high quality diesel fuel, whereas low molecular weight alkenes are favoured by high temperature operation [64]. The slurry reactor is used for the synthesis of gasoline from coal [65].

Another type of reactor is the circulating fluidised bed (CFB) reactor. This reactor is mainly used for HTFT. This reactor has an advantage in that it is easy to replace the used catalyst online. The reactor temperature is controlled by means of heat exchangers in the reactor.

Sasol commissioned a fixed fluidised bed (FFB) reactor in 1990 [66].The reactor is much simpler to run, a lot less complex and smaller than the circulating fixed bed reactors as shown in Figure 4. Due to the nature of the reactor itself, it provides high oil selectivity and higher conversions than that obtained for an equivalent CFB reactor [67].

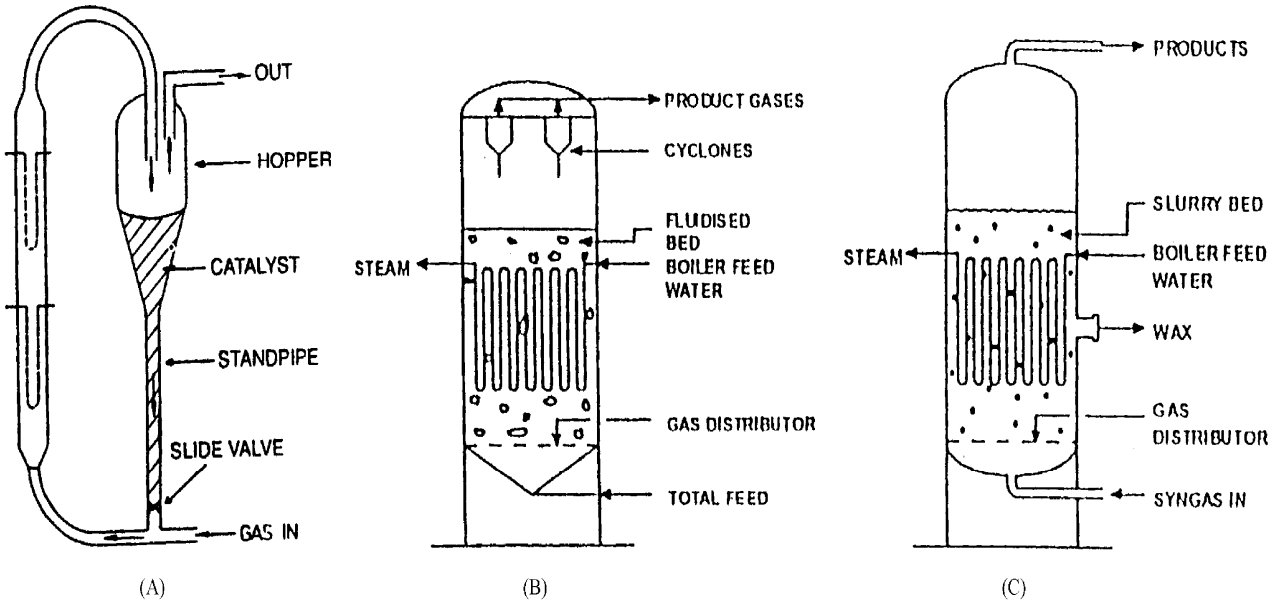


Figure 1.4: Fluidised bed FT reactors: (A) CFB reactor; (B) ebulating or FFB reactor; (C) Slurry phase bubbling bed reactor, Types (A) and (B) are two phase systems (gas and solid catalyst), while type (C) has three phases present, gas passing through a liquid in which the solid particle catalyst are suspended. Note the diagrams are not drawn to the same scale. The CFB reactors are about three times higher than the FFB or slurry reactors. [60]

1.6.3. Fisher-Tropsch catalysts

Several types of catalysts can be used for FT Synthesis. The most important ones are based on iron or cobalt. Cobalt catalysts have the advantage of generating a high conversion rate and they have a long life time. The Co catalysts are in principle more reactive for hydrogenation and therefore produce less unsaturated hydrocarbons and alcohols compared with iron catalysts.

Iron catalysts have a higher tolerance for sulphur, are very cheap and produce more olefin and alcohol products. The life time of the iron catalysts are, however, very short (about eight weeks) [68]. Iron based catalysts produce mostly normal paraffinic and alpha-olefinic hydrocarbons and a smaller quantity of oxygenate such as normal alcohols [69]. Most of the water formed as a product is converted to carbon dioxide and hydrogen by the water gas shift reaction (WGS).

Most studies on FT catalysts have been carried out with the metals supported on silica, alumina, or titania. In recent years, other families of supports with a carbonaceous base in the form of activated carbon and CNTs have been investigated for FT reactions [61]. Activated carbon has many advantages if utilised as a FTS catalyst support (resistance to acidic or basic media, stable at high temperatures, etc). CNTs possess similar properties and in most cases outperform activated carbon for FTS. CNTs as a new type of carbon material have interesting properties favouring catalytic activity. Their special structural characteristics and morphology are quite suitable for use as catalytic support materials [70].

1.6.4. Promoter effects

Promoters are doping agents added to catalyst materials in small amounts to improve their activity, selectivity, and/or stability [71]. It is generally accepted that promoter elements may induce these beneficial effects in several ways. The way of controlling the product selectivity in FT reaction is to introduce promoters into the catalyst and is considered as a component of the catalyst that does not take part in a catalytic reaction but changes the properties of the catalyst. There are two types of promoters usually employed for improving the Fe catalysts in FTS, chemical and structural promoters. Structural promoter can improve a catalyst's structural features by enhancing its surface area while maintaining its stability in a catalytic reaction. Chemical promoters affect the catalysts electronic in nature. This occur as a result of a change in the electronic environment of the catalyst surface, and can lead to enhanced reactant gas active site interactions which can lead to bonding destabilization of the reactant gas [72]. All this has led researchers to come up with a classification scheme for promoter effects. Although promoter elements are not considered themselves to be catalytically active, they may play other roles under FT catalytic conditions. This is highlighted for the Fe catalyst used in FT synthesis. Potassium, for example, produces an increase in the formation of alkenes and decreases the yield of methane while copper decreases the temperature of the iron reduction reaction [73]. A survey of the literature has revealed a number of studies in which promoters have been used to enhance the activity of Fe for MWCNT synthesis [74-76].

The data obtained in this study can be compared and contrasted to literature reports on related systems. In particular two papers have appeared since this work was commenced that have bearing on the results obtained in this study. To summarize. A consideration of the project objectives can be seen on the Table below.

Table 1.2: Comparison of data for the synthesis of CNTs produced from this study and similar literature studies.

Catalyst	Temperature regime		
	<350°C	300-500°C	>500°C
Fe	FT regime	Qi et al. [77]	This study[a]
Fe-Cu	FT regime	Qi et al. [77]	This study
Fe-K	FT regime	-	This study
Fe-Co/K	FT regime	-	Balogh et al. [78]

[a]Many studies by others have also been performed on Fe catalysed CNT production.

Qi et al [77] cover a different temperature regime than that investigated in this study, while the study by Balogh et al. [78] covers a K content different from that used in this study. Even the Cu content used by Balogh et al. [78] is different to that used in this study.

Balogh et al. [78] study the influence of K on the production of different shaped carbons , in particular CNTs was investigated over a Co/Fe catalyst. Different Co/Fe ratios were used. Specific conclusions revealed from the study were:

1) When different KA salts [A = NO_3, CH_3COO, IO_3, CO_3, $(COO)_2$, $CO(CH_3)$] were used the anion, A, influenced the CNT yield. Their results revealed that A= IO_3 and $(COO)_2$ were able to increase activity and give yields even higher than produced over A= NO_3.

2) The optimum K content was found to be 3% K by mass (relative to Fe).

In this study only $Fe(NO_3)_2$ was used as an Fe source so direct comparison with Balogh et al.'s [4] results can be made. However then this study showed that as the K content increased, the CNT yield decreased.

The conclusion reached is that:

The effect of K on Fe in the FT reaction , K is known to lead to higher olefin content in the production stream, suggesting a less hydrogenating catalyst. This same phenomenon seems to hold at the higher temperature, even though the product is different. In this study as the temperature increased from 600˚C-700˚C the yield of the product decreased over the Fe catalyst.

Qi et al [77] synthesised Fe/Cu catalysts and investigated their effect on the synthesis of shaped carbon materials. The Fe:Cu ratios used was 1:10 which is not a typical ratio used in FT studies or in this study. In this study a Fe:Cu ratio of 10: 0.6 was used , values normally used in FT studies. As a consequence in the Qi et al [77] study the influence of Cu will dominate over that of Fe and hence carbon will be produced that is more typical of the presence of Cu than of Fe.

Furthermore the temperature regime used to make the carbon nanotubes was 400-500˚C, which is between FT and CNT synthesis temperatures (See Table 7). They observed high yields of carbons with shapes dominated by carbon nanobelts and helical tubes. The catalyst reduction was carried out at 400, 450 and 500˚C (4 h reaction) and the reduction temperature played a large role in both yields and carbon structure produced. Their study also revealed that when only Fe was used, no carbon nanobelts were formed, and high yields of helical CNTs were produced. When only Cu was used some helical carbons and belt like carbon nanofibers were produced. It

was also noted that temperature played a significant role in the formation of products produced. The diameters of the nanotubes ranges between 80 nm–100 nm.

Munga et al [79] studied the effect of catalyst promotion on the FT synthesis of Fe/CNT catalyst promotion and they revealed that the unpromoted iron supported on CNTs produces a very stable and active catalyst. The effect of K on Fe in the FT reaction, K leads to decreased hydrogenation and increased chain growth, producing higher molecular weight products. Also the production of C_2 olefins increased and the methane production decreases while WGS activity increases. The effect of copper increases FT synthesis reaction rate but did not have a major effect on the production spectrum.

Tavasoli et al [80] studied FTS on CNT supported and alumina supported cobalt catalysts. They observed that using CNT as cobalt catalyst support causes the reduction temperature of cobalt oxide species to shift to lower temperatures and aided in well dispersion of metal clusters size decreased. CNT caused a slight decreased in the FT product distribution to lower molecular weight hydrocarbons.

In this study the influence of the Cu on the Fe is apparent. Instead of straight CNTs, coiling dominates. This is an expected feature when Cu is used to make shaped carbons [81]. The diameters are in 60 and 100 nm range for Fe and Fe-Cu respectively. Promotional effects of the Fe/CNT catalyst for FT synthesis were examined, K was found to increase the hydrocarbon yield and the CO conversion. The K promoted catalyst increased the CO reaction rate. Addition of K on Fe/CNT also increased the olefinity and the alpha value. Cu decreased the reduction temperature of ion oxides as noted by TPR studies. The Cu promoted catalyst showed a high selectivity to methane and a decrease of C_{5+}. The C_2 olefins also decreased.

1.7 Aims and objectives of this study

The objective of this project was to investigate the influence of Cu, K, Cu/K and SiO_2 as promoters for Fe in the synthesis of MWCNTs and to test this catalyst for FT synthesis.

(1) The effect of Cu and K promoters on Fe FT catalyst is well known. These reactions are performed at low temperatures (200-350^{o}C). Fe is an excellent catalyst used to synthesize CNTs at higher temperatures (600-1150^{o}C). The question then arises as to the impact of these promoters on Fe catalysts in the high temperature regime in the synthesis of CNTs.

(2) In particular the Cu should aid Fe reduction possibly leading to modified behaviour of the Fe catalyst (higher yields) for the synthesis of CNTs. Similarly the ability of K to produce longer chain hydrocarbons in the FT reaction could lead to modified CNT products. A SiO_2 containing catalyst should improve catalyst stability due to the strong Fe-SiO_2 interaction.

The specific aims of the project were the following:

(1) To synthesise CNTs over Fe/$CaCO_3$ catalyst and over Cu, K, Cu/K and SiO_2 promoted Fe/$CaCO_3$ catalysts.

(2) To provide basic characterization of all catalysts prepared using TEM, SEM, TGA, Raman spectroscopy, Brunauer-Emmett and Teller (BET) surface area, Energy dispersive X-ray (EDX), temperature programmed reduction (TPR) and inductive couple plasma (ICP-EOS).

(3) To use the CNTs produced as supports for Fe catalyst in FT synthesis.

This study should then provide further details on CNT synthesis as well as on carbon supported Fe FT catalysts.

1.8 References

[1] O'Connell M.J., Carbon nanotubes properties and application, CRC press, New York, 2006.

[2] www.mse.umd.edu/...final.../Carbon-Nanotubes-final-report-465-spr2003.pdf - (accessed on 25 March 2009).

[3] http://www.azonano.com/details.asp?ArticleID=982 (accessed on 10 October 2009).

[4] Wilson M, Nanotechnology: Basic Science and Emerging Technologies, Chapman and Hall/CRC, (2002).

[5] http://www.personal.rdg.ac.uk/~scsharip/tubes.htm (accessed on 13 October 2009).

[6] http://www.nanotech-now.com/nanotubes-buckyball-sites.htm (accessed on 15 October 2009).

[7] Cees D., Carbon nanotubes as molecular quantum wires, Physics Today **52** (5): (1999) 22.

[8] http://nanogloss.com/nanotubes/what-are-the-physical-properties-of-carbon-nanotubes

(accessed on 5 November 2009).

[9] http://www.nanotech-now.com/Carbon-Nanotubes-101.htm. (accessed on 15 June 2009).

[10] Trans S.J., Verschueren A.R.M., Dekker C., Nature **393** (1998) 49.

[11] Rueckes T., Kim K., Joselevich E., Tseng G.Y., Cheung C.-L., Lieber C.M., Science **289** (2000) 94.

[12] Bachtold A., Hadley P., Nakanishi T., Dekker C., Science **294** (2001) 1317.

[13] Liang W., Bockrath M., Bozovic D., Hafner J.H., Trinkham M., Park H., Nature **411** (2001) 665.

[14] Cheng H. M., Yang Q. H., Liu C., Carbon **39** (2001) 1447.

[15] Chambers A., Park C., Baker R.T.K., Rodriguez N.M., J. Phys. Chem. B **102** (1998) 4253.

[16] Park C., Anderson P.E., Chambers A., Tan C. D., Hidalgo R.J., Rodriguez N.M., J. Phys. Chem. B **103** (1999) 10572.

[17] Bahome M.C., Jewell L.L., Hildebrandt D., Glasser D., Coville N.J., Appl. Catal. A: Gen. **287** (2005) 60.

[18] Dai L., Carbon Nanotechnology, University of Dayton, Dayton, Ohio 45469-0240, USA, Elsevier, 2006.

[19] Robertson J, Mater. Today **10** (2007) 37.

[20] Trojanowicz M., Trend. Anal. Chem. **25** (2006) 480.

[21] Paradise M, Goswami T, Materials & Design **28** (2007) 1477.

[22] http://www.azonano.com/details.asp?ArticleID=980 (accessed on 10 October 2009).

[23] Wei B.Q, Appl. Phys. Lett. **79** (2001) 1172.

[24] Gao B, Chem. Phys. Lett.**32**7 (2000) 69.

[25] Ma R.Z, Science in China Series E-Technological Sciences **43** (2000) 178.

[26] http://www.cheaptubes.com/cntapplications.htm (accessed on 10 October 2009).

[27] Walters D, Chem. Phys. Lett.**338** (2001) 14.

[29] Baughman R.H., Science **290** (2000) 1310.

[30] Huang H., Kijuura H., Tsutsui S., Hirano Y., Miyakoshi M., Yamada A., Ata M., Chem. Phys. Lett. **343** (2001) 7.

[31] Ebbesen T.W., Ajayan P.M., Nature **358** (1992) 220.

[32] Seung J.L., Hong K.B., Jae-eun Y., Jong H.H., Diamond Relat. Mater. **11** (2002) 914.

[33] Guo T., Nikolaev P., Thess A., Colbert D.T., Smalley R.E., Chem. Phy. Lett. **243** (1995) 49.

[34] Guerrero A., Puerta J., Gomez F., Blanco F., Phys. Scr. T131 (2008) 014007 (4pp).

[35] Yudasaka M., Yamada R., Sensui N., Wilkins T., Ichihashi T., Iijima S, J., Phys. Chem. B **103** (1999) 6224.

[36] Park J.B, Choi G.S, Cho Y.S, Hong S.Y, Kim D, Choi S.Y, Lee J.H, Cho K.I, J. Cryst. **244** (2002) 211.

[37] Ivanov V, Nagy J.B, Lambin P, Lucas A, Zhang X.B, Zhang X.F, Bernaerts D, Van Tendeloo G, Amelinckx S, Van Landuyt J, Chem. Phys. Lett. **223 (**1994) 329.

[38] Hernadi K, Fonseca A, Nagy J.B, Fudala A, Baenaerts D, Lucas A, Zeolites **17** (1996) 416.

[39] Couteau E, Hernadi K, Seo J.W, Thiên-Nga L, Mikó Cs, Gaá1 R, Forró L, Chem. Phys. Lett. **378** (2002) 9.

[40] Duncan R, Stolojan V, Lekakou C, Proceedings of the World Congress on Engineering, London, (2007).

[41] Andrews R, Jacques D, Rao A.M, Derbyshire F, Qian D, Fan X, Dickey E.C, J. Chen, Chem. Phys. Lett. **303** (1999) 467.

[42] Cao A , Ci L, Wu G, Wei B, Xu C, Liang J, Wu D, Carbon **39** (2001) 152.

[43] Singh C, Shaffer M, Kinloch I, Windle A, Physica B **323** (2002) 339.

[44] Takenaka S, Ishida M, Serizawa M, Tanabe E , Otsuka K, J. Phys. Chem. B **108** (2004), 11464.

[45] Singh B.K, Ryu H, Chikate R.C, Hoa N.D, Park S.J, Kim S, Lee J.R, Solid State Commun. **139** (2006), 102.

[46] Iijima S, Nature, **354** (1991) 56.

[47] Huang H, Chem. Phy. Lett. **343** (2001) 7.

[48] http://en.wikipedia.org/wiki/carbon_nanotube. (accessed on 12 May 2009).

[49] Mhlanga S.D, Synthesis and Study of Carbon nanotubes and Spheres, PhD Thesis, University of Witwatersrand, Johannesburg, 2009.

[50] Yasuda A, Kawase N, and Mizutani W. Phys. Chem. B **106** (51), (2002) 13294.

[51] Belin T, Epron F, Mater. Sci. and Eng. B **119** (2005) 105.

[52] http://www.SiliconFarEast.com (accessed on 09 October 2009).

[53] http://www.si-mex.com.mx orton thermogravimetric analysis (accessed on 09 October 2009).

[54] Arepalli S, Nikolaev P, Gorelik O, Hadjiev V, Holmes W, Files B, Yowell L, Carbon **42** (2004) 1783.

[55] Ferrari A, Robertson J, Phys. Rev. B **61** (2000) 14095.

[56] Bahome M.C, Synthesis and use of carbon nanotubes as a support for the Fischer-Tropsch synthesis, PhD Thesis, University of the Witwatersrand, Johannesburg, 2007.

[57] Louer D, Mittemeijer E.J, Powder diffraction in materials science, 2000, Max Planck Institute for Metals Research, Seestrasse 92, 70174 Stuttgart, Germany.

[58] http://www.netl.doe.gov (accessed on 17 June 2009).

[59] Tavasoli A, Trepanier M, Abbaslou R.M.M, Dalai A.K, Fuel Process. Technol. (2009) doi:10.1016/j.fuproc.2009.07.007.

[60] Dry M.E, Catalysis Today **71** (2002) 233.

[61] Malek Abbaslou R.M, Tavasoli A, Soltan J, Dalai A.K, App. Catal. A: General **367** (2009) 47.

[62] Dry M.E. Appl. Catal. A: General **138** (1996) 319.

[63] Jager B. Espinoza R. Catal. Today **23** (1995) 17.

[64] (a) Adesina A.A, Appl. Catal. A: general **138** (1996) 345 (b) Eilers J, Posthuma S. A, Sie Catal. Lett. **7** (1997) 253.

[65] Rao V.U.S, Stiegel G.J, Cinquegrane G , Srivastava R.D., Fuel Proc. Tech. **30** (1992) 83.

[66] Jager B, Dry M.E, Shingles T and Steynberg A.P, Catal. Lett**. 7** (1990) 293.

[67] Dry M.E. Catalysis Today **6** (1990) 183.

[68] http://www.ecn.nl/biomassa/research/polyftsynthesis.en.html (accessed on 05 May 2009).

[69] Huff G.A, Jr and Satterfield C.N, Ind. Eng. Chem. Process. Des. Dev. **23** (1984) 696.

[70] Trepanier M, Tavasoli A, Dalai A.K, Abatzoglou N, Fuel Process.Technol. **90** (2009) 376.

[71] Cornils B, Heermann W.A, Schlogl R, Wong C.H, Catalysis from A-Z, A concise encyclopedia, Wiley-VCH,Weinhem, (2000).

[72] Hexane W.M, A systematic study of the effect of chemical promoters on the precipitated Fe based Fischer Tropsch Synthesis catalyst, PhD Thesis,University of Witwatersrand, Johannesburg, 2009.

[73] Bartholomew C. H, New Trends in CO Activation, Studies in Surface Science and Catalysis, No. 64, Elsevier Science Publishers, Amsterdam, (1991) 158.

[74] Balogh Z, Halasi G, Korbély B, Hernadi K, Appl. Catal. A: Gen. **344** (2008) 191.

[75] Cheng J, Zhang X, Luo Z, Liu F, Ye Y, Yin W, Liu W, Han Y, Mater. Chem. And Phys. **95** (2006) 5.

[76] Escobar M, Rubiolo G.H, Moreno M.S, Goyanes S, Candal R, Journal of Alloys and compound **479** (2009) 440.

[77] Kim S, Kim K, Ahn H, Cho K, J. Alloys and Compnd. **449** (2008) 274.

[78] Balogh Z, Halasi G, Korbély B and Hernadi K, Appl. Catal. A: Gen. **344** (2008) 191.

[79] Bahome M.C, Jewel L.L, Hildebrandt D, Glasser D, Coville N.J. Appl. Catal. A: General **287** (2005) 60.

[80] Tavasoli A, Sadagiani K, Khorashe F, Seifkordi A.A, Rohani A.A, Nakhaeipour A, Fuel Process. Technol. **89** (2008) 491.

[81] Qi X, Zhong W, Deng Y, Au C, Du Y, J. Phys. Chem. C **113** (2009) 15934.

Chapter 2

Experimental

2.1 Carbon nanotubes.

Carbon nanotubes (CNTs) were synthesized by chemical vapor deposition (CVD). Among the different methods of synthesising carbon nanotubes i.e. electric arc discharge [1], laser ablation [2] and chemical vapour deposition [3-6], the chemical vapour deposition method seems to be the most promising, in particular in terms of large scale industrial applications. This is due to the relatively easy possibility to upscale both the preparation and the purification methods [7, 8]. The method has certain advantages such as giving high yields and controllable growth conditions. CVD synthesis using a $CaCO_3$ catalyst support can overcome the difficulties of catalytic CNT production. $CaCO_3$ is a nonporous material where the formation of carbon does not occur in pores during the nanotube growth and therefore selective formation of CNTs is promoted. The advantage of using $CaCO_3$ as catalyst support is the decomposition of $CaCO_3$ into CaO and CO_2 at the reaction temperature. Hence, after multiwalled carbon nanotubes synthesis the main by-product is CaO, which is soluble in dilute acids. This simplifies the purification procedure considerably [9]

2.1.1 Preparation of catalysts

The catalysts were prepared using the incipient wetness impregnation method [10]. $Fe(NO_3)_3.9H_2O$, $Cu(NO_3)_2.3H_2O$ and KNO_3 were used as precursors. All chemicals were purchased from MERCK Chemicals (PTY) LTD. The $Fe(NO_3)_3.9H_2O$ precursor was used as a source of iron (dissolved in 30 ml distilled H_2O) and was added dropwise onto the $CaCO_3$ support to give the desired 10 wt % loading of Fe on the support. The promoted Fe catalysts were prepared by dissolving $Fe(NO_3)_3.9H_2O$ and KNO_3(0.4%K) or $Fe(NO_3)_3.9H_2O$ and Cu $(NO_3)_2.6H_2O$ (0.6% Cu) or $Fe(NO_3)_3.9H_2O$ in 30 ml distilled H_2O. Tetraethyl orthosilane (TEOS) was added in 2ml distilled water. These solutions were also added dropwise to the $CaCO_3$ support. The amount of K promoter was varied from 0.2, 0.3, 0.4, 0.5, and 1 % and Cu

from 0.4, 0.6, 1 and 2 %. After impregnation of the $CaCO_3$ support, the solutions were stirred for 2 hour and filtered to produce slurry which was oven dried overnight at 120 ºC. The dried slurry was ground, sieved and calcined at 400 ºC in air for 16 hour.

2.1.2 Synthesis of carbon nanotubes (CNTs)

The CNTs were prepared by the decomposition of acetylene (C_2H_2) (Afrox PTY LTD) using the CVD method. Catalyst 0.5 g was added to a quartz boat (120 mm x 15 mm) which was horizontally placed in the centre of a quartz tube reactor (51 cm x 1.9 cm i.d.). The quartz tube reactor was placed in a temperature controlled furnace. This furnace was electronically controlled making it possible to control the heating rate, reaction temperature and gas flow rates.

The catalyst was activated by passing N_2 (Afrox PTY LTD) through the reactor for 1 hour at a flow rate of 40 ml/min. After 1 hour had lapsed acetylene (C_2H_2) and N_2 were introduced into the reactor at flow rates of 90 ml/min and 240 ml/min respectively. The reaction was allowed to continue for 1 hour at a specific reaction temperature. Reaction temperatures investigated were 700 ºC, 750 ºC, 800 ºC and 850 ºC. The nitrogen gas was replaced with hydrogen at a flow rate of 100 ml/min. The reaction temperatures used were 700^0C, 800^0C, and 900^0C. Hydrogen was first used to activate the catalyst at a flow rate of 40 ml/min. and hydrogen gas flow rate was increased to 100 ml/min simultaneously with acetylene at flow rate of 100 ml/min for 1 hour.

The C_2H_2 flow was stopped after 1 h and the furnace was left to cool down to room temperature under a N_2 flow (40 ml/min) and under H_2 in the case of the reaction that was reduced by hydrogen. The black carbon material (CNTs and armophous carbon) deposited onto the boat was then weighed.

The differences in mechanism of activation of N_2 and H_2 are the quality and the yield of the CNTs produced under N_2 was found to be excellent compared to those produced under H_2 (figure 23).

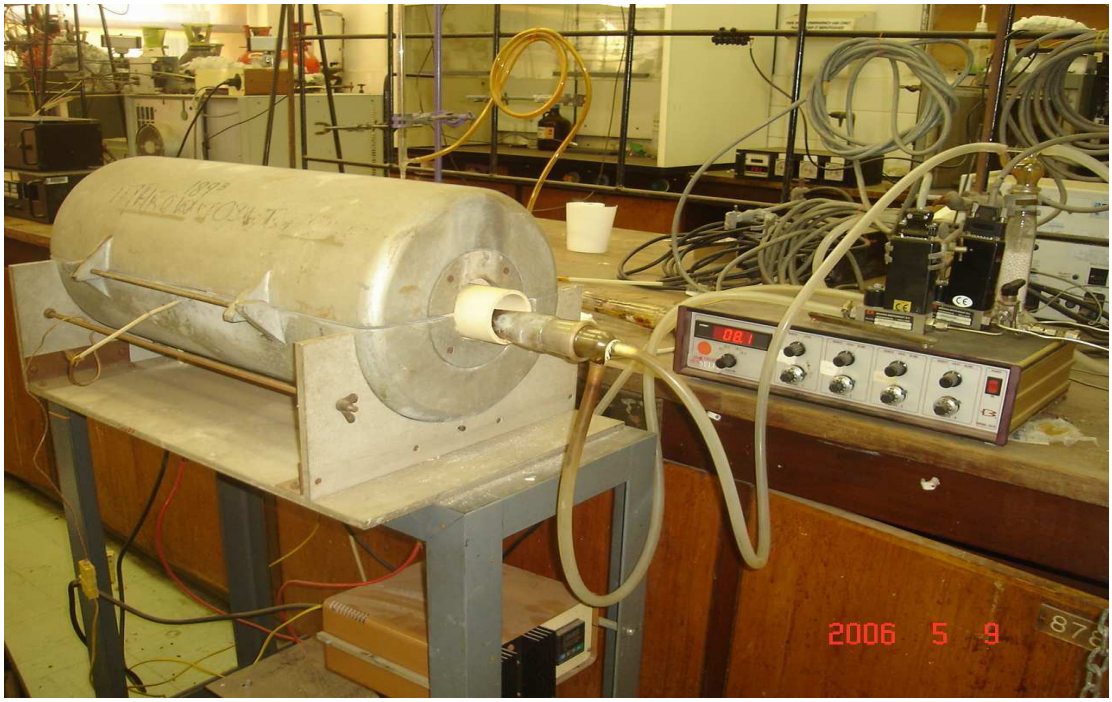


Figure 2.1: CVD setup used for the synthesis of CNTs

2.1.3 Purification of carbon nanotubes

Purification mainly involves the separation and removal of catalyst particles, support material and armophous carbon from CNTs. A 30% (HNO_3) nitric acid solution was used to purify the carbon nanotube product. The carbon nanotubes were washed by stirring vigorously in excess 30% nitric acid (HNO_3) for 2 hours at room temperature. The material was recovered by filtration, thoroughly washed with distilled water until neutral and finally dried in an oven at 120°C overnight. Hence the one step chemical treatment is simple and does not affect the CNTs structure (see figure 3.26). No residual CaO was trapped after acid treatment.

2.2 Fisher-Tropsch

The Fischer-Tropsch (F-T) reaction converts a mixture of hydrogen and carbon monoxide to liquid fuels. The Fischer-Tropsch process was discovered by German scientists in the 1920's and used to make fuels during World War II. There has been continued interest of varying intensity in Fischer-Tropsch technology ever since that time. The Fischer-Tropsch reaction is used commercially to synthesise clean liquid fuels from synthesis gas (syngas). The Fischer-Tropsch syngas conversion can be achieved with catalysts based on Fe, Co and Ru [11].

2.2.1 Synthesis of catalysts supported on CNTs

2.2.2 Preparation of Catalysts.

The Fe catalyst was prepared by the incipient wetness impregnation method. A 10% Fe solution made from $Fe(NO_3)_3.9H_2O$ dissolved in 4.5 ml de-ionised water was added drop-wise to 2.5 g purified carbon nanotubes support. The promoted iron catalyst was prepared by adding 0.6%Cu from $Cu(NO_3)_3.3H_2O$, 0.4%K from KNO_3 respectively to the iron solution prepared above and the mixture added drop-wise to 2.5 g of the carbon nanotube support. The slurry was dried overnight in an oven and calcined in nitrogen at 220˚C for 2.5 hours.

2.2.3 Fisher-Tropsch synthesis

Synthesis of Fischer-Tropsch products was carried out in a fixed bed micro-reactor [12]. Gas cylinders containing $H_2/CO/N_2$ mixtures (30%CO, 60%H_2, and 10% N_2) were used to supply the reactant gas stream to the catalyst. Nitrogen was used as an internal standard in order to ensure an accurate mass balance. The hydrocarbon product areas were corrected for olefins and paraffins by using response factors based to those used by Dietz [13], and Scanlon et al. [14]. The mole fraction of hydrocarbons $X_{HC,\,i}$ was calculated as.

$$X_{HC,\,i} = \left(\frac{RFi \,.AHC,i}{Ac2,cal}\right) X_{c2,\,cal}$$

Where RF_i is the response factor for carbon number i , $A_{HC,\,i,}$ is the integrated GC area for a hydrocarbon with carbon number i , $A_{c2,\,cal}$ and $X_{c2,\,cal}$ refer to peak area and mole fraction of the C_2 hydrocarbon in the calibration gas [15].

The % CO conversion was calculated as: $\left[\frac{COin - COout}{CO\,in} Nin/Nout\right] *100$

Where CO_{in} is the area of the CO peak in the feed, CO_{out} is the area of the CO peak in the gaseous product stream, $N_{2,in}$ is the area of the nitrogen peak in the feed and N_2, out is the area of the nitrogen peak in the product stream.

The product selectivity for hydrocarbons S_i was calculated for component X_i as follows:

$$S_i = \left[\frac{mass\ component\ Xi}{\Sigma Xi}\right] * 100\%$$

The olefin to paraffin ratio X_2 was given as:

$$X_2 = \frac{mass\ olefin\ X2}{\text{total hydrocarbon mass } X2}$$

About 0.5 g catalyst was added to the reactor and reduced in situ at 350 °C for 24 h under a stream of pure hydrogen (2 bar pressure, 20 ml/minute). After reduction the temperature was decreased to 275 °C, synthesis gas was introduced, and the pressure was increased gradually to 8 bar. All gas lines after the reaction were kept at 150 °C and the hot trap placed immediately after the reaction was held at 150 °C in order to collect wax. A second trap kept at ambient temperature was used to collect the oil and water mixture.

The product stream was analyzed online using two gas chromatographs. The thermal conductivity detector (TCD) was used to analyze H_2, N_2, CO, CO_2 and CH_4 and was calibrated using a calibration gas mixture with a 30%CO, 60%H_2, and 10% N_2 composition. Before FT reactions, carbon monoxide and hydrogen were allowed to bypass the reactor. The peak areas obtained from bypass were used to calculate the number of moles of each component going into

the reactor. During FT reaction, injections were done for both TCD (H_2, CO, CH_4 and CO_2 analysis) and FID (hydrocarbons analysis) online.

The first peak on TCD was identified as hydrogen peak and both areas of hydrogen in the calibration gas and in gaseous product stream were integrated. Argon was used as an internal standard and the H_2 signal was big enough to do a quantitative analysis. The flame ionization detector (FID) was used for the analysis of hydrocarbons and was calibrated with a calibration gas in order to identify the hydrocarbon peaks [16].

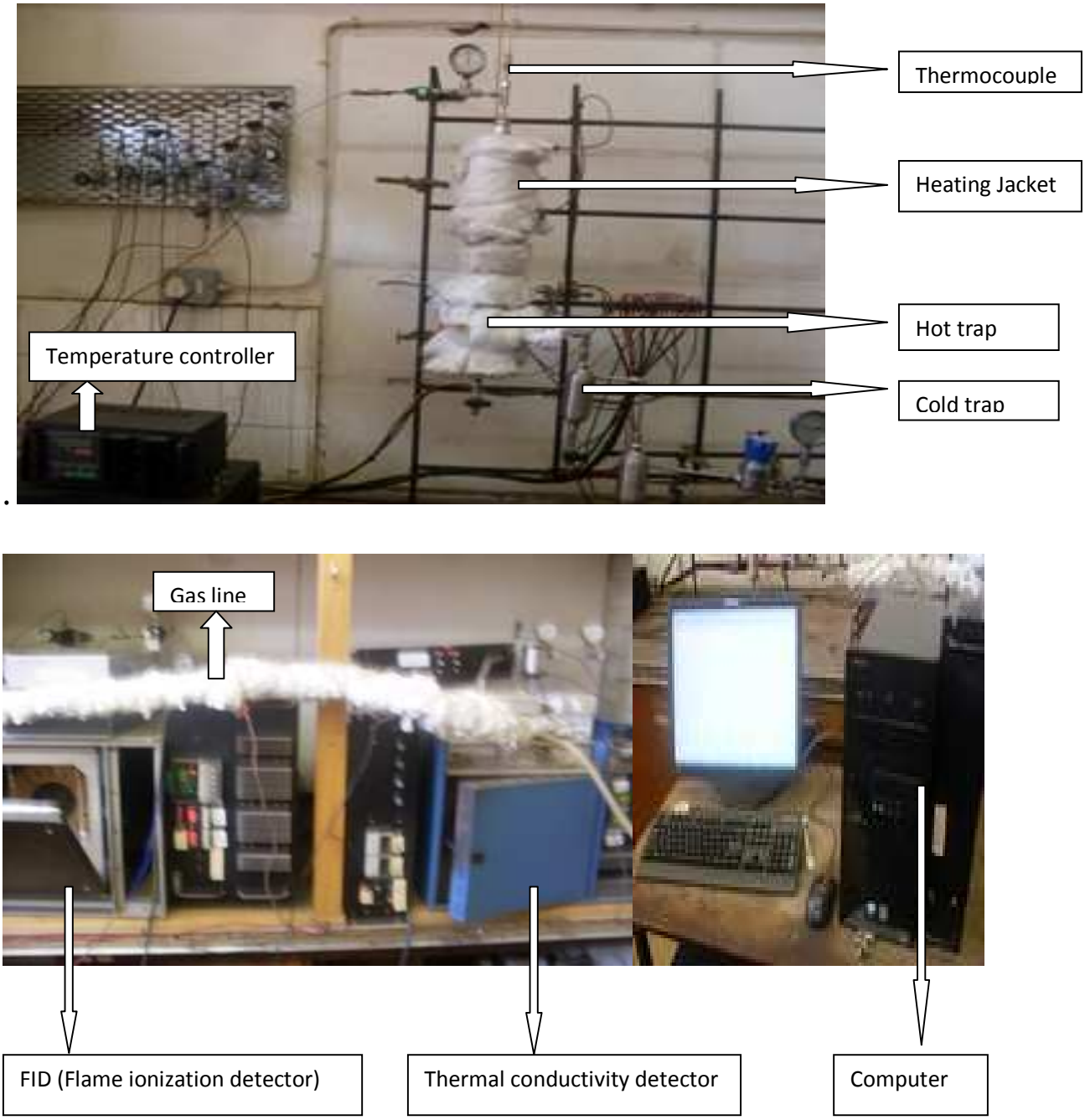


Figure 2.2: F-T reactor with temperature controller, FID, TCD and Computer.

2.3 Characterisation techniques

2.3.1 N_2 Physisorption

N_2 physisorption was employed for the surface-area determination and pore volume measurements of all the Fe catalysts. The samples were degassed using N_2 at 150 ºC for 6 hours before measurement. N_2 adsorption-desorption isotherms at N_2 boiling point (-196 ºC) were measured on a Micromeritics TRISTAR 3000 analyzer. The surface areas were determined by the Brunauer-Emmett-Teller (BET) method [17].

2.3.2 Transmission electron microscopy (TEM)

TEM was employed to verify the yield, the wall structure and the purity of carbon nanotubes produced. A small amount of the sample was sonicated in a water bath for 10 minutes and methanol was added to each sample. The sample was added dropwise to a copper-grid, allowed to dry and it was then ready to be viewed under a FEI TECNAI SPIRIT electron microscope.

2.3.3 Thermogravemetric analysis (TGA)

TGA was performed with a Perkin Elmer STA 6000 analyzer to monitor the weight loss of the carbon nanotubes, the thermal stability and the decomposition temperature of the samples. The temperature of the samples was increased at a rate of 10ºC/min from 29 to 900ºC under air flow of 20 ml/min.

2.3.4 Raman Spectroscopy

Raman spectroscopy (SENTERRA) at laser wavelength = 532 nm was employed to show the graphitic layers and disorder bands in the carbon nanotubes. The ratio between the D and G bands is a good indicator of the quality of the bulk samples. If the intensity of these both bands are similar this indicates a high quantity of structural defects.

2.3.5 Scanning electron microscopy (SEM)

SEM analysis was carried out using a JSM-840 scanning microscope that images the sample surface by scanning it with a high-energy beam of electrons in a raster scan pattern. The electrons interact with the atoms that make up the sample producing signals that contain information about the sample's surface topography, composition and other properties such as electrical conductivity.

2.3.6 Energy dispersive X-ray (EDX)

EDX is a technique used for identifying the elemental composition of the specimen and was carried out using a FEI TECNAI SPIRIT (TEM-EDX) electron microscope. An EDX spectrum plot not only identifies the element corresponding to each of its peaks, but the type of X-ray to which it corresponds as well. Each of the peaks is unique to an atom, and therefore corresponds to a single element. The larger the peak intensity in a spectrum, the more concentrated the element is in the specimen, once the cross section factors have been applied.

2.3.7 Temperature programmed reduction (TPR)

The temperature-programmed reduction (TPR) experiment was performed on 0.1 g sample in a Micromeritics AutoChem11 Chemisorption Analyser model equipment, using a 5% H_2/Ar gas mixture. Before the analysis, the samples were heated under an argon flow (20 ml min^{-1}) at 10 °C min^{-1} until 150 °C for 30 min. Then a temperature programme allowed the temperature to be ramped linearly from room temperature to 800°C under a flow of 5% H_2 balanced in argon.

2.3.8 Inductive Coupled Plasma-Optical Emission Spectroscopy (ICP-OES)

Inductively Coupled Plasma Optical Emission Spectroscopy (SPECTRO GENESIS) was used for obtaining the elemental analysis of a material and the metal loading on the support. In this technique, the determination of trace concentrations of elements in a sample was achieved using atomic emission spectroscopy.

2.4 References

[1] Journet C. and Bernier P., Appl. Phys. A **67**(1998) 1.

[2] Journet C., Maser W.K., Bernier P., Loiseau A., Lamy de la chapelle M., Lefrant S., Deniard P., Lee R and Fischer J.E , Nature **388** (1997) 756.

[3] Thess A, Lee R, Nikolaev P, Dai H, Petit P, Robert J, Xu C, Hee Lee Y, Gon Kim S, Rinzler A.G, Colbert D.T, Scuseria G.E , Tomanek D, Fischer J.E and Smalley R.E Science **273** (1996) 483.

[4] Hernadi K, Fonseca A, Nagy J.B, Sisko A and Kiricsi I, Appl. Cata. A **199** (2000) 425.

[5] Colomer J.F, Stephan S, Lefrant S, Van Tendeloo G, Willems I, Konya Z, Fonseca A, Laurent Ch. and Nagy J.B , Chem. Phys. Lett. **317** (2000) 83.

[6] Basca R.R, Laurent C.H, Peigney A, Bacsa W.S, Vaugien T.H and Rousset A ,Chem. Phys. Lett. **323** (2000) 566.

[7] Li W.Z, Xie S.S, Qian L.X, Chang B.H, Zou B.S, Zhou W.Y, Zhao R.A and Wang G , Science **274** (1996) 1701.

[8] Vanadan V.K and Xie J, Smart Mater. Struct. **11** (2002) 728.

[9] Couteau E, Hernadi K, Seo J.W, Thien-Nga L, Miko Cs, Gaal R, Forro L, Chem. Phys. Lett. **378** (2002) 9-13.

[10] Bahome M.C, Jewell L.L, Hildebrandt D, Glasser D, Coville N.J, Appl. Catal. A: Gen. **287** (2005) 60.

[11] www.netl.doe.gov/publications/factsheets/rd/R&D089.pdf (17 June 2008)

[12] Dry M.E. Appl. Catal. A: General **138** (1996) 319.

[13]. Dietz, A.W. J. Gas Chrom. (1967) 62

[14]. Scanlon, J.T., Willis, D.E. J. Chrom. Sci. 23 (1985) 333

[15]. Mokoena, E. M. Synthsis and use of silica materials as support for the Fischer-Tropsch reaction, PhD Thesis, University of the Witwatersrand, Johannesburg, 2005.

[16] Bahome M.C. Synthesis and use of carbon nanotubes as a support for the Fischer-Tropsch synthesis, PhD Thesis, University of the Witwatersrand, Johannesburg, 2007.

[17] Idakiev V, Yuan Z.Y, Tabakova T. Su b.l, Appl.Catal. A: Gen. **281** (2005) 149.

Chapter 3
CNTs Synthesis
Results and Discussion

3.1 Introduction

Carbon nanotubes (CNTs) can be produced using a wide range of catalysts [1-5] as well as templates [6]. Indeed their production, ranging from the milligram to multigram scale can be regarded as straight forward and conventional. Notwithstanding, there are still issues of purity, chirality and type of CNT that are not controllable in most of the procedures that have developed over time. As the production of CNTs has now moved from the era of exploration, this control has become the focus of attention.

It is well known in the field of catalysis that promoters can assist in catalytic reactions. Promoters are generally broken down into two types: structural and electronic [7]. The role of a promoter is to "fine tune" a catalyst. In Fischer-Tropsch (FT) synthesis the metals of importance from an industrial perspective are Fe and Co. Many reviews and publications have been written on catalyst use in FT synthesis and the role of these catalysts in converting syngas ($CO + H_2$) to fuels and chemicals. Further, the standard Fe and Co commercial catalysts are now known to contain specific promoters that aid the FT reaction. The Fe FT catalyst is typically promoted by Cu, K, and SiO_2. The catalyst is typically operated at $T < 350^oC$ and the impact of these promoters in the FT reaction in this temperature regime is well established. As mentioned in chapter 1, CNTs can readily be made using Fe as catalyst. This then leads to an interesting question: Can the well known promoters that are used in Fe catalyzed FT catalysis influence the behavior of the Fe catalyst used to make CNTs. The reaction conditions are clearly different viz FT catalysts operate at $T < 350^oC$ and CNT production occurs at $600^oC < T < 900^oC$. However, in both regimes carbon deposits do occur and there may be parallels between the two processes.

This chapter is then taken up with the synthesis and characterization of CNTs produced in the presence of Cu, K and SiO_2 promoters. In the following chapter these same CNTs were used as catalyst supports for FT catalysis. Further the Fe/CNT catalyst was promoted with Cu, K and Cu/K for use in FT catalysis.

In terms of prior studies by others, little has been reported on the role of the promotion of Fe catalyst by Cu and K in CNT synthesis. After this study was commenced a report did appear by Balogh and co-workers [4] in which K doped Fe was used as a catalyst for CNT synthesis. Comparisons of the results obtained here with the study reported by Balogh et al. [4] will be made in the discussion. In principle the results from this study are in agreement with that reported by Balogh et al. In terms of prior studies on the promotion of Fe/CNT catalysts by Cu, K, and Cu/K there have been reports by Bahome [8], van Steen [9], Hayakawa [10], etc. Again the new results (Chapter 4) reported here will be contrasted with reports that have previously appeared.

In summary. The results include the effect of promoters (Cu, K, SiO_2) on the synthesis of carbon nanotubes over an iron catalyst. A number of characterisation techniques were employed to study the effect of promoters on iron catalysts. In all cases, the promoted and unpromoted catalyst produced a black product. Prior to analysis the carbon material was treated with 30% HNO_3 (and 10% HF for the SiO_2 containing catalyst) by stirring the product vigorously in excess acid for 2 hours at room temperature. The carbon was then washed until the pH of the washings was approximately 7.0. The washing removed the catalysts and promoters fron the CNTs.

The physical properties of CNTs synthesized with promoters were compared to those obtained when using the unpromoted Fe catalyst. The various amounts of promoters loaded onto the catalyst at different temperatures used for the synthesis of carbon nanotubes is also reported. A temperature of 600^oC was found to be an optimum temperature for loading CNTs with 0.4% K and 0.6% Cu. These same loadings of both K and Cu were used to promote iron catalyst supported on carbon nanotubes for Fischer-Tropsch synthesis.

3.1.1 Effect of copper (Cu) on carbon nanotube production

A Fe/Cu catalyst was used to synthesise CNTs. In preliminary studies the temperature was varied from 600-900°C and 600°C was found to give the optimal yield of CNTs with the 0.6% Cu promoted catalyst (see section 3.1.6) on page 58. The reaction entailed passage of acetylene over the Fe/Cu on $CaCO_3$ catalyst (Chapter 2 for details) for 1 hour. After acid treatment the black carbonaceous material was analysed.

(i) Electron microscopy (TEM and SEM) analysis

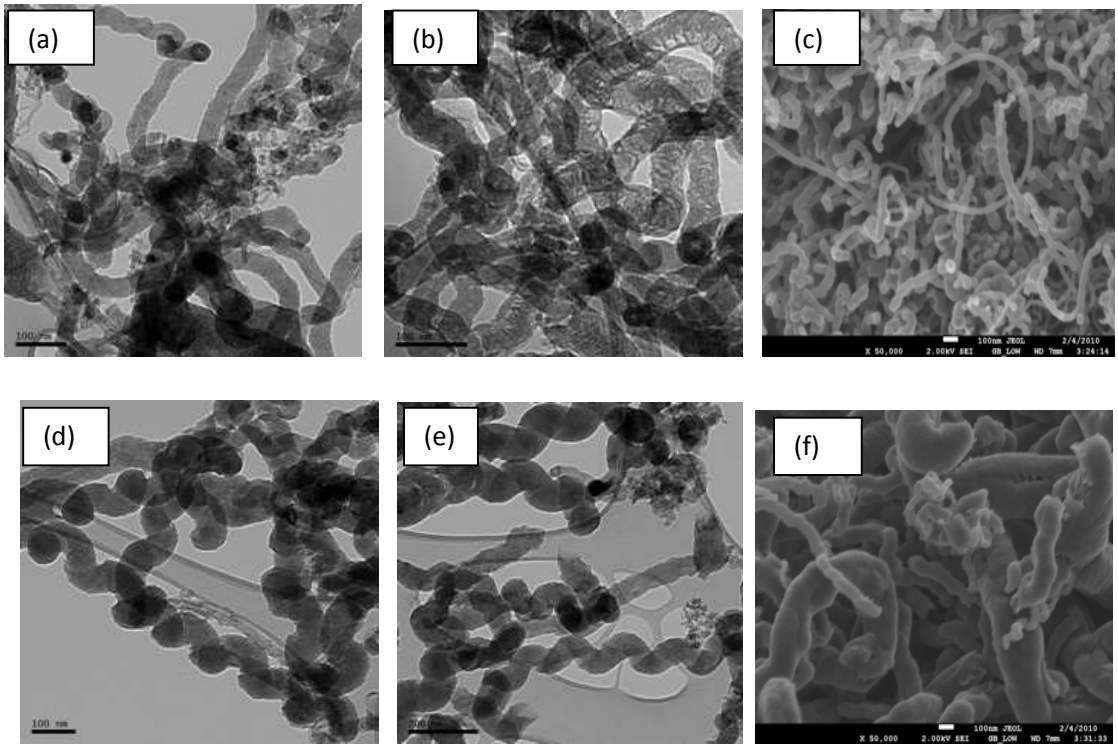
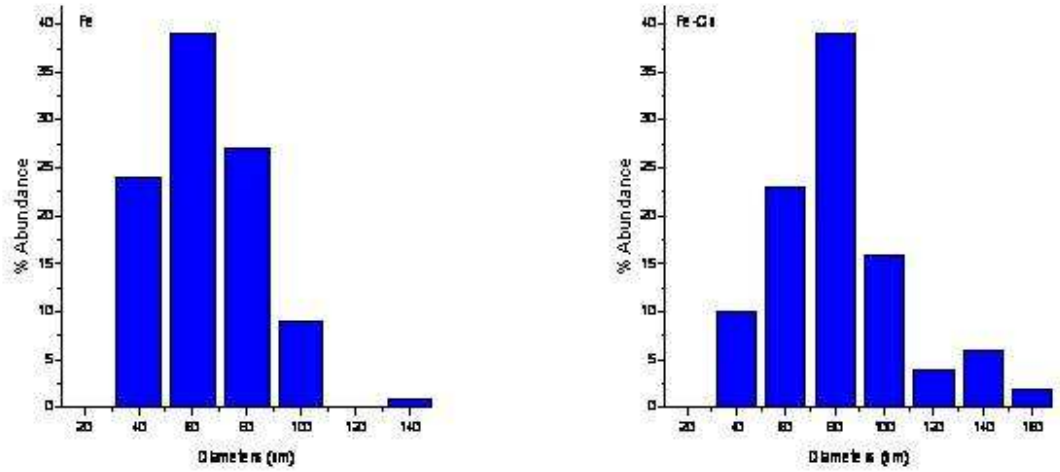


Figure 3.1: TEM and SEM images of the product produced from Fe (a), (b), (c), and Fe-Cu (d), (e), (f) catalysts at 600°C for 1 hour.

TEM and SEM images of the product produced from the Fe and Fe-Cu on $CaCO_3$ support is shown in Figure 1. Figure 2 show that the unpromoted catalyst produced CNTs the majority of which had a diameter of 60 nm. Addition of a small amount of Cu (0.6%) to the Fe increased the yield and the diameter was also increased to 80 nm. The implication of this result is that the Fe particles are larger in the Fe/Cu catalyst leading to the larger diameter CNTs [11]. Fe particles could melt and agglomerate, creating larger particles than observed for the original catalyst. The non-agglomerating characteristic of Fe_2O_3 facilitates growth of thin CNTs [12].

There was no amorphous carbon observed in the purified carbon nanotubes. Iron particles were observed inside the carbon nanotubes in both the Fe and Fe/Cu materials. No particles were observed in the tips of the carbon nanotubes which indicate that there is a strong interaction between Fe metal particles and the CaO support and that a base growth mechanism is operating to produce the CNTs [13].

The most important difference between the products produced from Fe or Fe/Cu relates to the morphology of the CNTs produced by the different catalysts. The small amount of Cu introduced a higher degree of coiling in the CNTs (see Fig.1). The effect of Cu on CNT production has been extensively reported in the literature [14] and Cu at low temperature (< 400^{o}C) produces high yield of coiled CNFs. The percentage of coiled CNTs compared with straight CNTs in the product is approximately 90%. The yield of unpromoted Fe is 2.27 g and the promoted Fe is 4.04 g. Earlier it has been observed that CNTs prepared at a temperature around 700^{o}C have a straight morphology. This morphology change of the CNTs is due to a variation in the catalyst shape at different synthesis temperatures [15]



Figurer 3.2: Diameter distribution of the products produced from (a) Fe (b) Fe-Cu catalyst at 600ºC

(ii) EDX Spectrum

The EDX spectrum (Figure 3) confirmed that there was no Cu left behind after purification of the carbon nanotubes with acid. It also confirmed the presence of iron. The presence of titanium is related to the Ti grid.

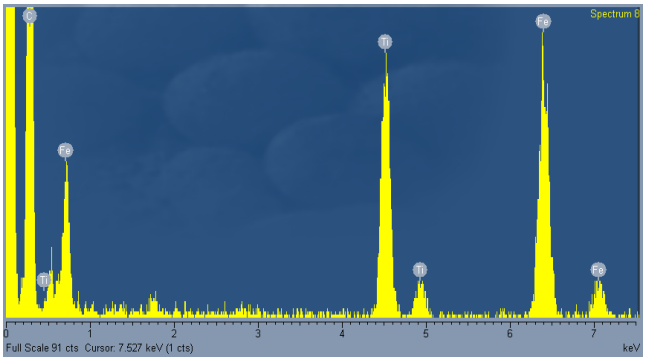


Figure 3.3: EDX spectrum of purified Fe-Cu CNTs

(iii) BET analysis

The surface area of carbon nanotubes that contained Cu is higher than that of the unpromoted catalyst (Figure 4). The specific surface area of unpromoted catalyst was found to be 85 m^2/g and the pore volume of 0.190 cm^2/g. The surface area of the promoted iron catalyst was 100 m^2/g with a pore volume of 0.225 cm^2/g. This modest increase could be associated with the coiling of the CNTs.

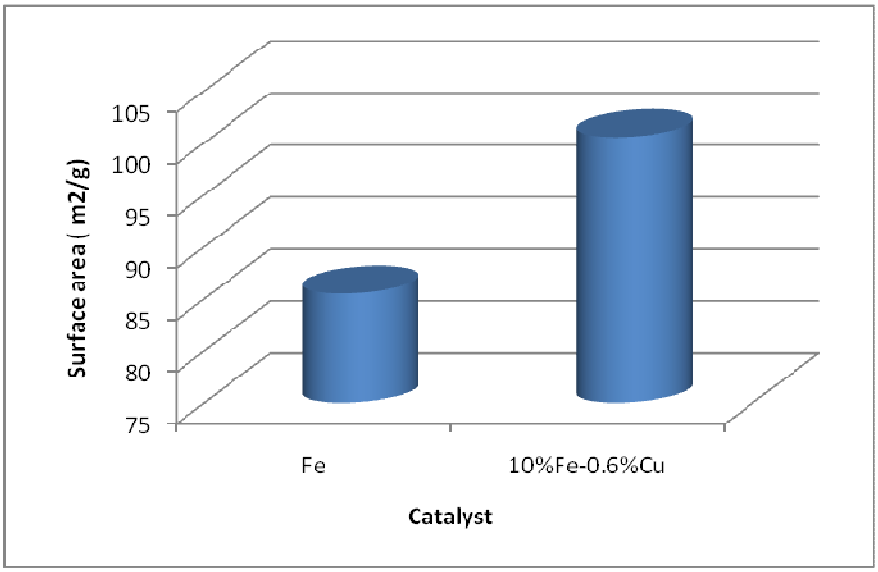


Figure 3.4: Surface area for Fe and Fe-Cu CNTs

(iv) Raman spectra

Structural features of the purified CNTs were studied by Raman spectroscopy. The typical analysis involves a comparison of two Raman active bands, called the D and G bands that are associated with the graphene structure of carbons. The D band is associated with "disorder" i.e with sp^3 type carbon atom while the G band is associated with the classic sp^2 bonding in carbon.

The band at 1592.3 cm^{-1}corresponds to the G mode i.e to the movement in the opposite direction of two neighbour carbon atoms in a graphite sheet [16]. The 1334.8 cm^{-1} band is assigned to the D mode. The intensity ratio, I_D/I_G is known to depend on the structural characteristics of CNTs and gives a measure of the tube quality. The larger the I_D/I_G value the poorer the quality of the CNT structure suggestive of a higher degree of disorder i.e more defects [17].

The Raman spectra for the two samples are given in Figure 5 and Table 1. The I_D/I_G values are equal to 1.3 and 1.1 for the Fe and Fe/Cu produced materials respectively. The lower I_D/I_G value for the Fe/Cu sample indicates that the extent of disorder in the CNTs has increased relative to the samples produced using the unpromoted $Fe/CaCO_3$ catalyst.

Table 3.1: ***Peak positions and the intensity ratio data (I_D/I_G) for the purified samples (a) Fe (b) Fe-Cu***

Sample name	Position	Intensity	Bandwidth	Integral	Line shape [a]	I_D/I_G	RMS[b]
Fe	1334.8	48.158	142.49	10778	100%Lorentz+Gauss	1.3	2.17
	1592.3	36.656	72.50	4174	100%Lorentz+Gauss		
Fe/Cu	1337.5	19.136	258.86	7780	100%Lorentz+Gauss	1.1	1.76
	1587.7	17.398	81.14	2217	100%Lorentz+Gauss		

[a] Line shape is the shape of the band, [b]RMS stands for root mean square ,this is the standard deviation of the curve fitting

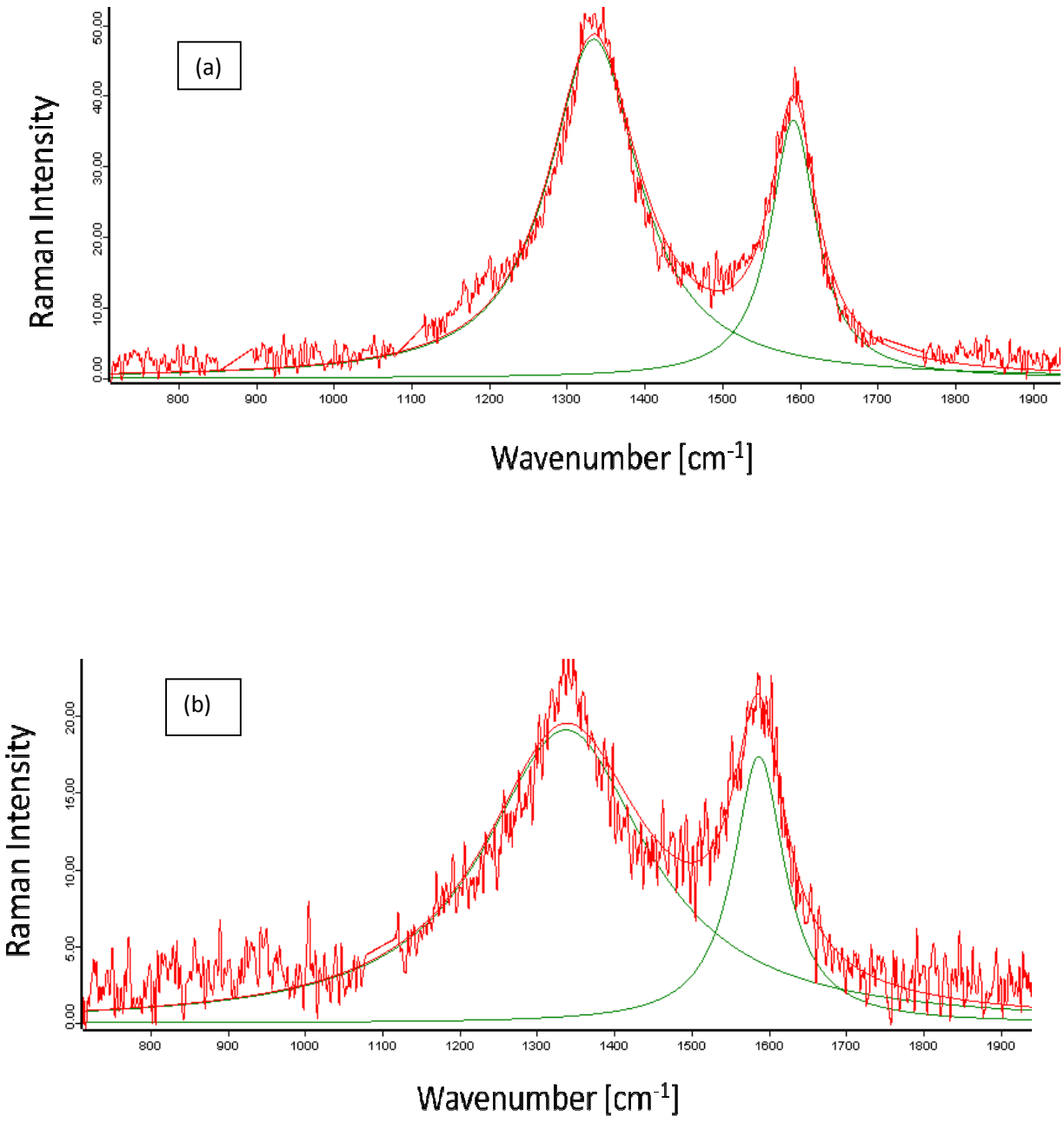


Figure 3.5: Raman spectra of (a) 10% Fe (b) 10%Fe-0.6%Cu materials.

3.1.2 Effect of potassium (K) on carbon nanotube production

The synthesis of CNTs using a 0.4% K on Fe catalyst supported on $CaCO_3$ is reported below. The reaction was performed at 600°C (acetylene as carbon source) and yields are reported after 1 hour of reaction. (See section 3.1.6 for choice of reaction conditions).

(i) Electron microscopy (TEM and SEM) analysis

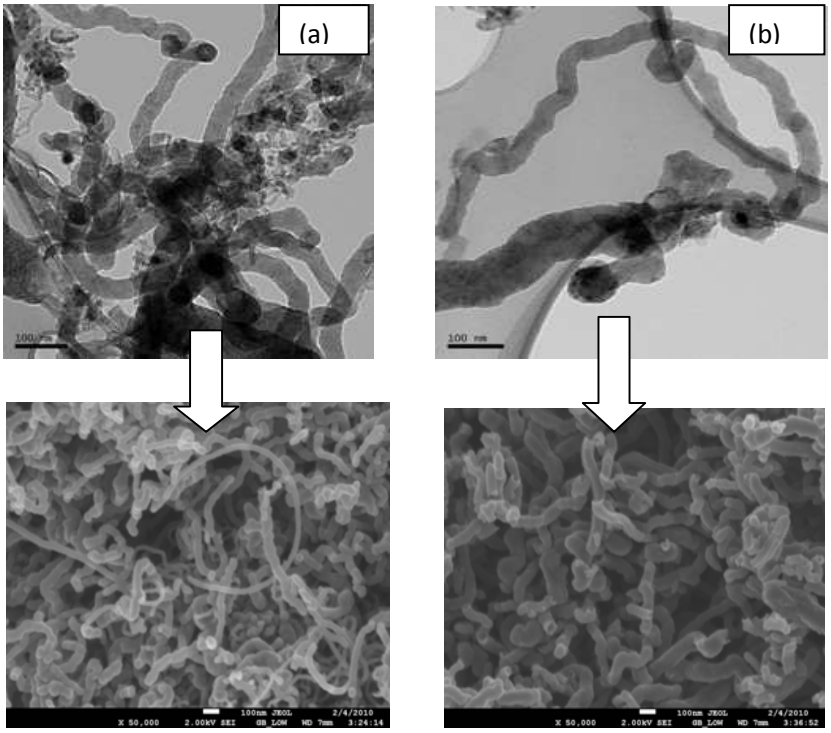


Figure 3.6: TEM and SEM images of the product produced from (a) Fe and (b) Fe-K catalyst at 600°C

TEM images revealed that the potassium promoted catalyst produced a mixture of CNTs and carbon nanofibers (CNFs) .The percentage of CNTs compared with CNFs is approximately 50%.

The average diameter of the CNTs produced over the Fe/K catalyst was on average 100 nm. Compared to the Fe catalyst the diameter has increased by use of a Fe/K catalyst (Figure 7). The yield also increased from 2.27g to 3.26 g. Potassium appears to improve the catalytic activity of the Fe for the CVD synthesis of carbon nanotubes [4]. There was no amorphous carbon observed in the purified carbon nanotube sample. Iron particles were also observed for both materials inside the carbon nanotubes.

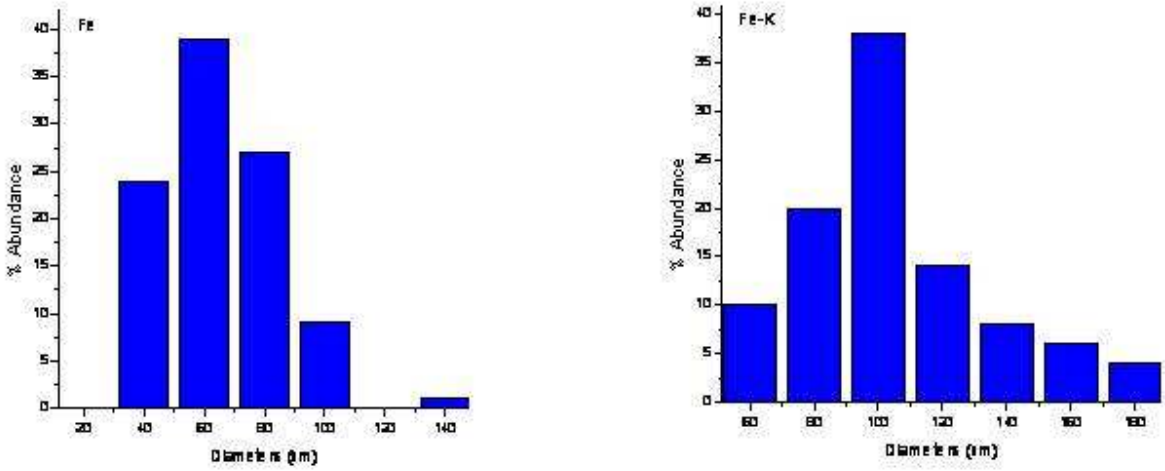


Figure 3.7: Diameter distribution of the product produced from (a) Fe (b) Fe-K catalysts at 600ºC

(ii) EDX analysis

The EDX spectrum shown in Figure 8 confirmed that there was no detectable potassium left behind after purification of the carbon naotubes. The EDX confirms the presence of residual iron. The copper peak is due to the use of a Cu grid.

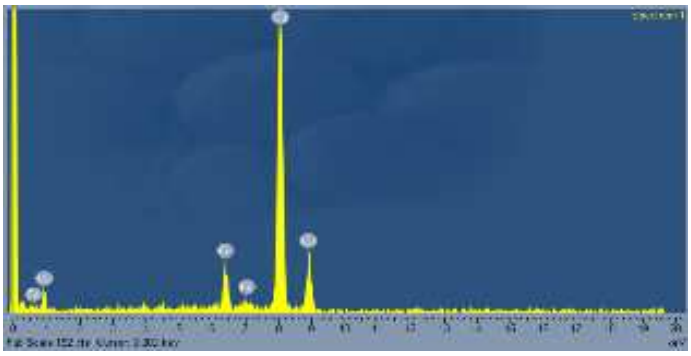


Figure 3.8: EDX spectrum of purified Fe-K CNTs

(iii) BET analysis

The surface area of carbon nanotubes that were produced from Fe/K is less than that of the unpromoted catalyst. Figure 9 shows that the surface area decreased for the carbon nanotubes produced from the promoted catalyst. The results indicated that the BET surface area decreased with increase in diameter of the MWCNTs [18].

The specific surface area of the unpromoted catalyst was found to be 85 m^2/g and the pore volume 0.190 cm^3/g. However that of the promoted iron catalyst was 47 m^2/g with pore volume equal to 0.14 cm^3/g. This suggests that the addition of potassium leads to blocking of the pores of this material.

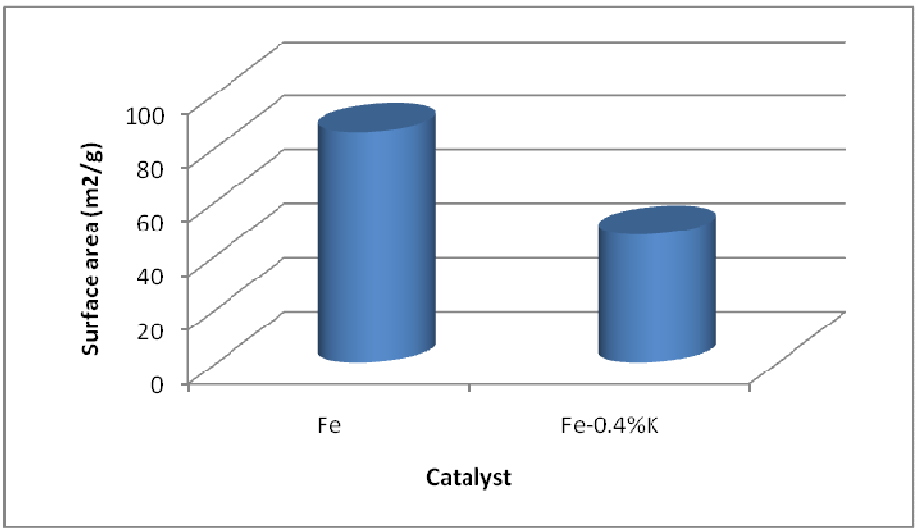


Figure 3.9: Surface area for Fe and Fe-K CNTs

(iv) Raman spectra

The I_D/I_G ratio, as mentioned in section 3.1.1 ,(iv) was measured to evaluate the graphitic nature of the CNTs produced over the Fe/K catalyst.

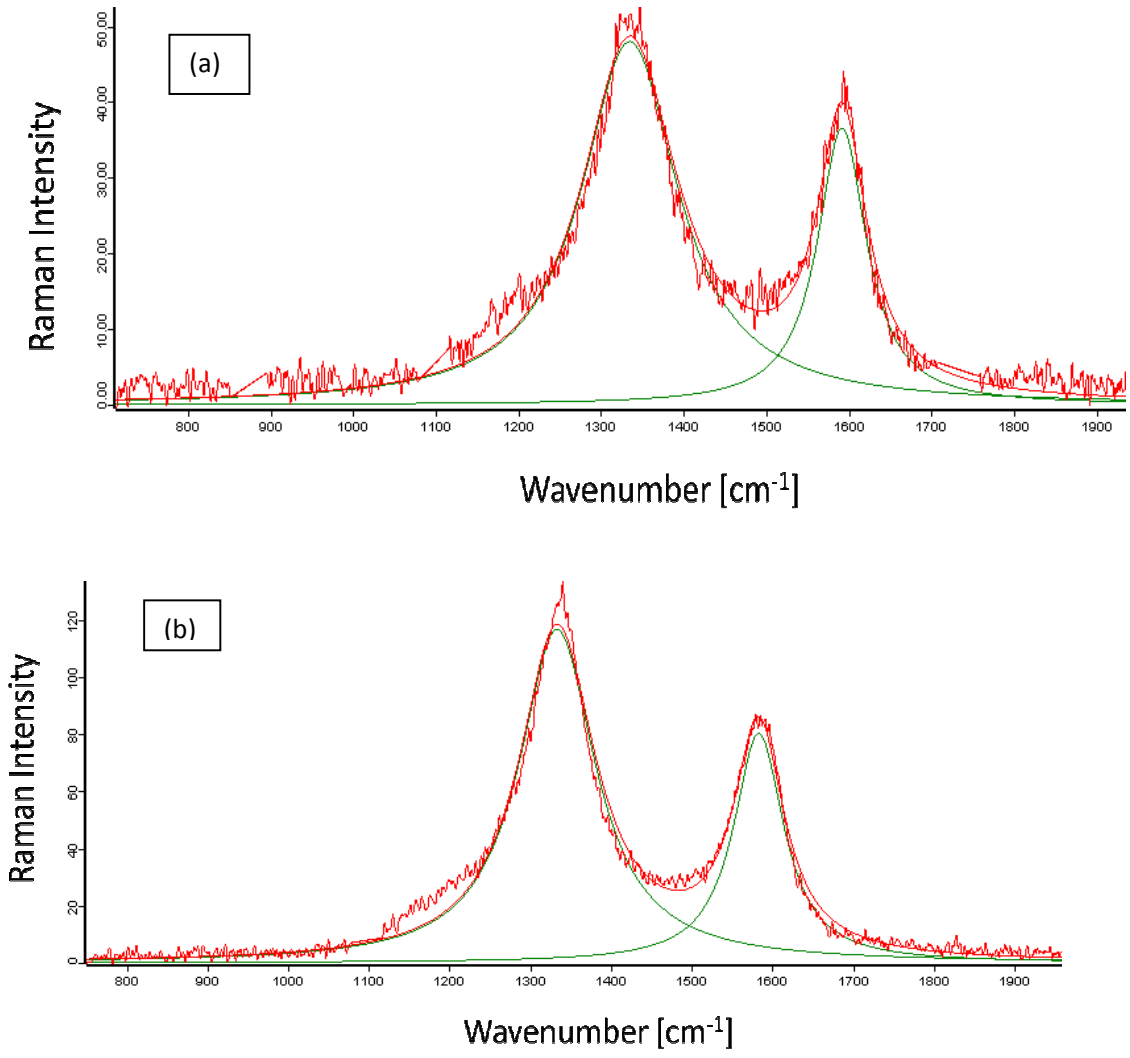


Figure 3.10: Raman spectra of (a) 10% Fe (b) 10%Fe-0.4%K materials

The D and G band for the Fe/K sample is shown in Figure 10 and data listed in Table 2. The I_D/I_G values are equal to 1.3 and 1.5 for the Fe and Fe/K samples respectively which suggests a greater degree of graphitization in CNT structures produced from the Fe/K catalyst. The position of the G band is shifted from 1592.3 to 1583.4 due to the addition of K.

Table 3.2: ***Peak positions and intensity ratios for the purified samples (a) Fe (b) Fe-K .***

Sample name	Position	Intensity	Bandwidth	Intergral	Line shape[a]	I_D/I_G	RMS[b]
Fe	1334.8	48.158	142.49	10778	100%Lorentz+Gauss	1.3	2.17
	1592.3	36.656	72.50	4174	100%Lorentz+Gauss		
Fe/K	1333.3	117.11	115.86	21314	100%Lorentz+Gauss	1.5	3.68
	1583.4	80.65	76.16	9649	100%Lorentz+Gauss		

[a] Line shape is the shape of the band, RMS[b] stands for root mean square, this is the standard deviation of the curve fitting.

3.1.3 Effect of co-addition of copper and potassium to $Fe/CaCO_3$

Many promoters are known to have cooperative effects. That is, the addition of two promoters can have a different effect than expected from knowledge of the effect of the separate promoter effects. To explore this issue, a catalyst comprissing of 0.6% Cu, 0.4% K added to $Fe/CaCO_3$ was synthesized. This catalyst was used to make CNTs from acetylene at 600^0C. The reaction was carried out for 1 hour.

(i) Electron microscopy TEM analysis

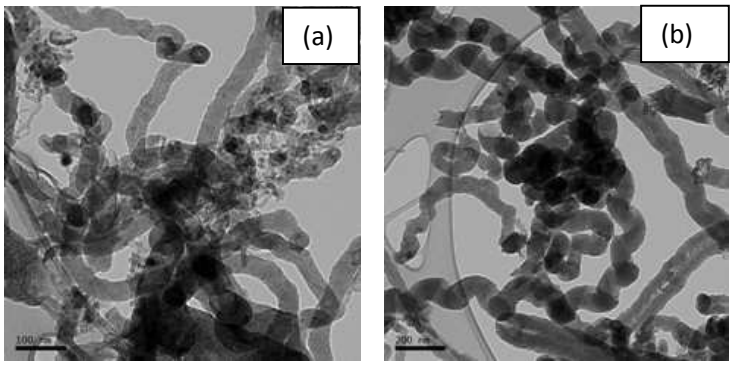
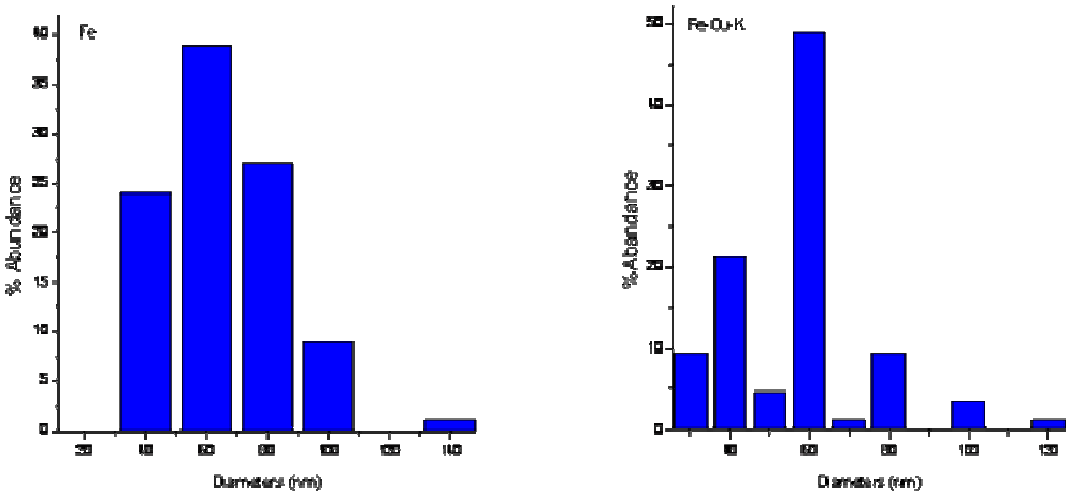


Figure 3.11: TEM images of the product produced from (a) Fe (b) Fe-K-Cu catalyst at 600ºC

TEM analysis of the purified products produced from the Fe and Fe-Cu-K on $CaCO_3$ support is shown in Figure 11.The bar graphs showing the average diameters of the CNTs produced by the two catalysts is shown in Figure 12. The unpromoted catalyst produced CNTs with a diameter of 60 nm, while the Cu/K promoted catalyst also produced CNTs with diameters of 60 nm. However, the CNT diameter distribution was quiete different for the two catalysts, and is different from the data produced from the separate use of the promoters (Figures 2, 7). Addition of a small amount of Cu (0.6%) and K (0.4%) to Fe also increased the yield of the CNTs from 2.27 g to 2.98 g. There was no amorphous carbon observed in the purified carbon nanotubes sample. Iron particles were observed inside the carbon nanotubes while Cu and K were washed away by 30% diluted HNO_3. The wider range of diameters suggests that the catalyst is most probably heterogeneous in composition. Thus, a simple mixing of the promoters did not simple produce a CNT sample with diameter ranging between 60-80 nm. The data rather suggest that the Fe particles are smaller than expected from the predictive effect. The morphology of Fe/Cu/K CNTs is coiled meaning they look more like the product produced from Fe/Cu CNTs. Thus the Cu promoter has the dominant effect in determining the CNT morphology.



Figurer 3.12: Diameter distribution of the products produced from the (a) Fe (b) Fe-Cu-K catalysts at 600ºC

(iii) BET analysis

The surface area of carbon nanotubes that were produced from the catalyst that contained both Cu and K is less than that of the unpromoted catalyst. Figure 9 shows that the surface area decreased for the product produced over the promoted catalyst. The specific surface area of product produced over the unpromoted catalyst was found to be 85 m^2/g with pore volume of 0.190 cm^3/g, however that of the promoted iron catalyst was 74 m^2/g with pore volume of 0.335 cm^3/g. It should be remembered that the Fe/K catalyst also showed a similar effect, whereas the Fe/Cu catalyst had a higher surface area. Thus, the K plays a more significant role in affecting the CNT surface area than does Cu.

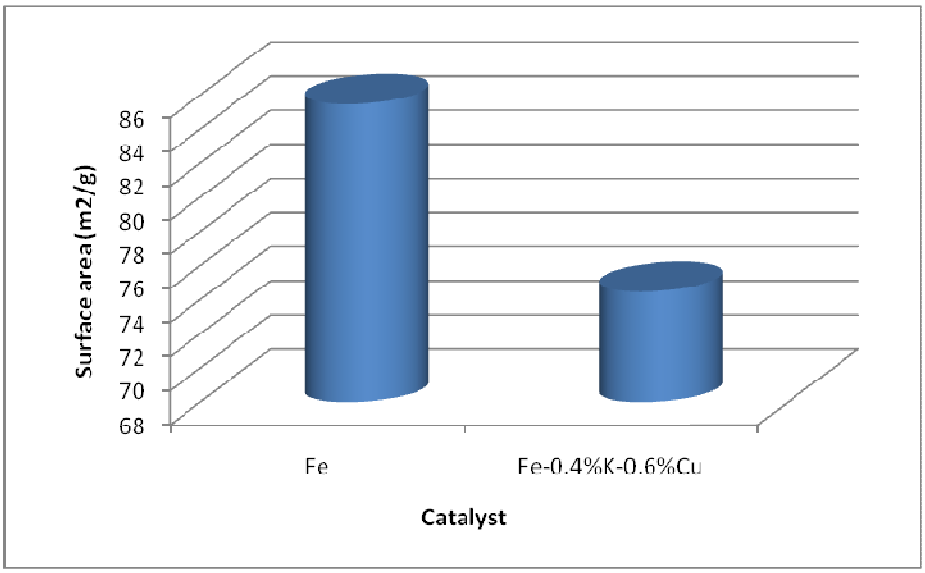


Figure 3.13: Surface area for Fe and Fe-K-Cu CNTs

(iv) Raman analysis

The Raman spectrum of the CNTs produced from the Fe/K/Cu was recorded (Figure 14). The D and G band positions and intensities were measured. The I_G/I_D ratios (Table 3) indicate a high quantity of structural defects. The I_D/I_G values were 1.3 and 1.0 for the Fe and Fe/Cu/K samples respectively which suggests a lower degree of graphitization in the CNTs produced with the promoter. It is clear that the effect of the two promoters on the Raman spectrum is similar to that of the use of either promoter used separately. However the shape of the Raman D band looks more like that of the Cu promoted sample**.** The position of the D band is shifted up while the G band is shifted down for the CNTs produced on the Fe/K/Cu/$CaCO_3$ catalyst.

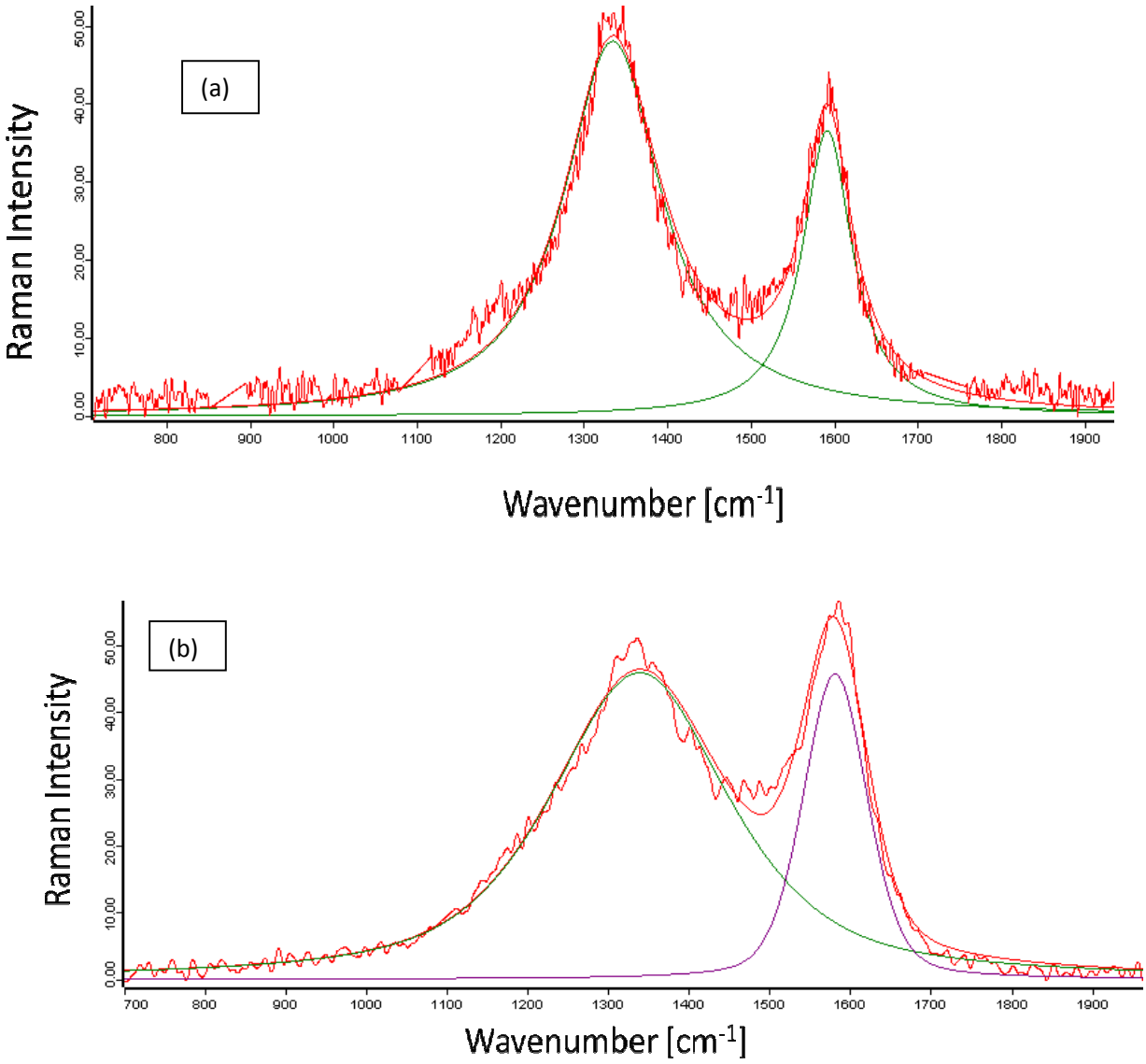


Figure 3.14: Raman spectra of (a) 10% Fe (b) 10%Fe-0.6%Cu/0.4%K material

Table 3.3: ***Peak positions of the purified samples (a) Fe (b) Fe-Cu-K and the intensity ratio of the bands.***

Sample name	Position	Intensity	Bandwidth	Integral	Line shape[a]	I_D/I_G	RMS[b]
Fe	1334.83	48.158	142.49	10778	100%Lorentz+Gauss	1.3	2.17
	1592.27	36.656	72.50	4174	100%Lorentz+Gauss		
Fe/Cu/K	1338.85	46.087	264.19	17103	100%Lorentz+Gauss	1.0	1.68
	1581.68	45.890	94.20	5279	100%Lorentz+Gauss		

[a] Line shape is the shape of the band, [b]RMS stands for root mean square, and this is the standard deviation of the fitting.

3.1.4 Effect of SiO_2 on carbon nanotubes production.

The use of SiO_2 as a promoter was also explored. TEOS was used as the SiO_2 source and Si addition was achieved by adding 0.1 ml of TEOS in 2 ml of water. The mixture was added to $Fe/CaCO_3$. CNTs were produced over the Fe/SiO_2 catalyst supported on $CaCO_3$ from acetylene at 600°C for 1 hour. The SiO_2 was removed from the carbon deposit after reaction by use of 10% HF. TEM analysis of the carbon material both unpromoted and promoted indicated the change in the diameter distribution of the CNTs.

(i) Electron microscopy TEM Analysis

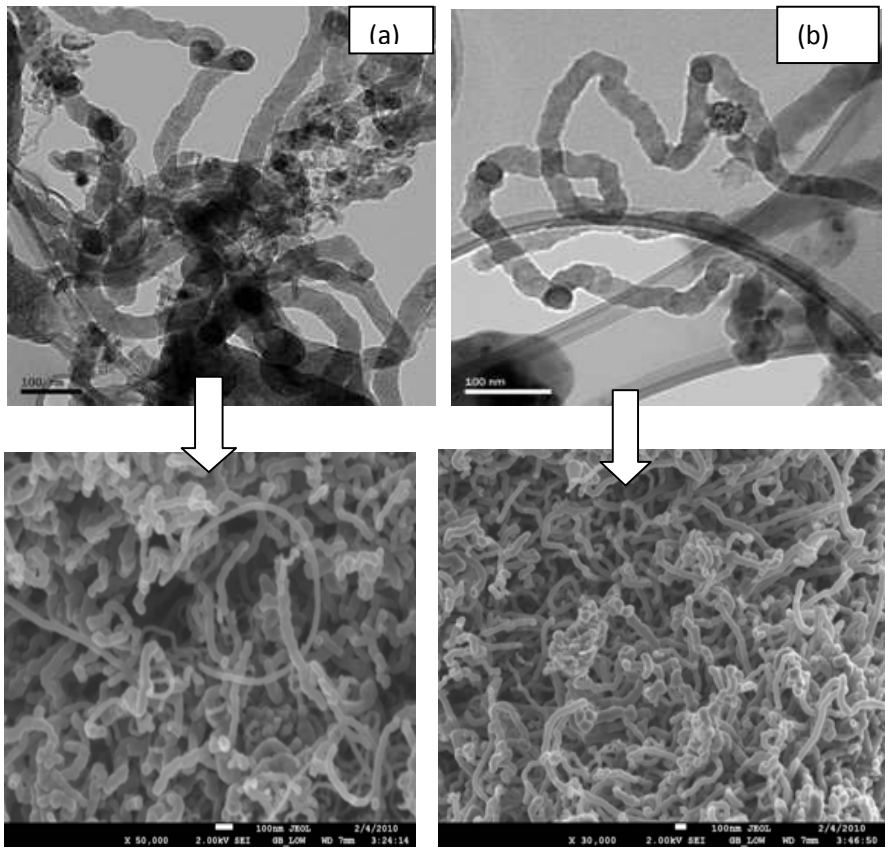


Figure 3.15: TEM and SEM images of the product produced from (a) Fe and (b) Fe-SiO_2 catalyst at 600ºC

TEM and SEM images of the catalyst are shown in Figure 15. The average diameter of the CNTs is much larger than those produced over the unpromoted CNTs (Figure 16). Addition of a small amount of SiO_2 to Fe decreased the yield of the CNTs from 2.27 g to 1.55 g. The bar diagram shows a CNT diameter distribution that is heterogeneous which in turn suggests that a range of Fe particle sizes occur in this catalyst.

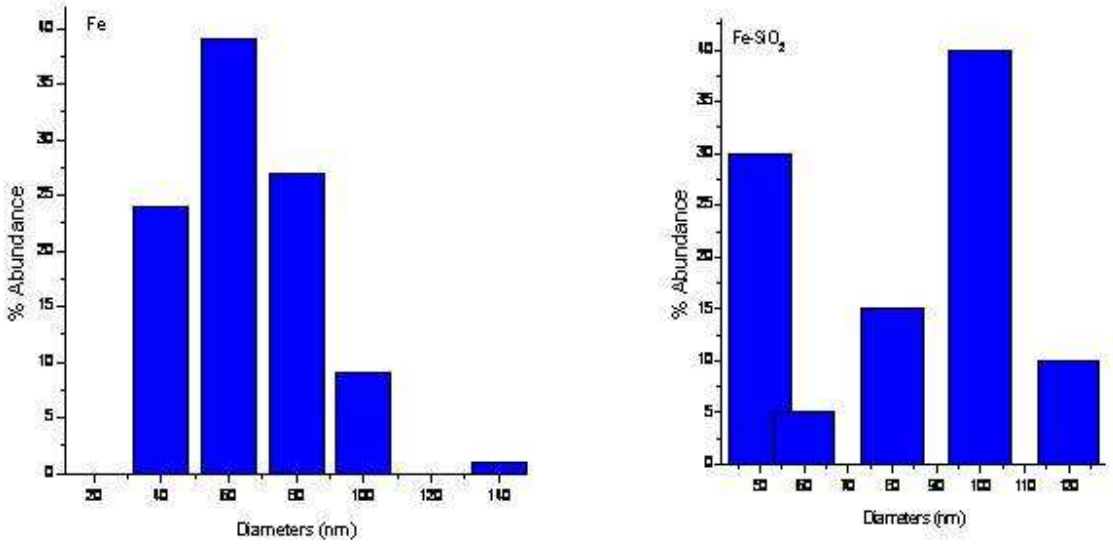


Figure 3.16: Diameter distribution of the product produced from (a) Fe-SiO_2 (a) Fe catalyst at 600ºC

(ii) EDX analysis

The spectrum in Figure 17 confirmed that there was no detectable SiO_2 that was left behind after purification of the carbon nanotubes. The EDX spectrum confirms the presence of iron.

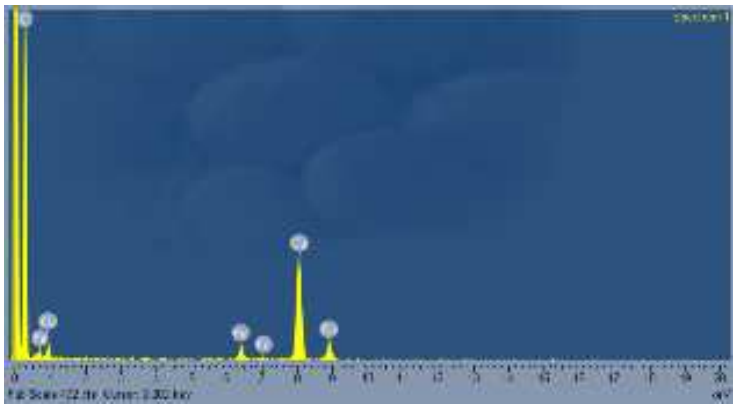


Figure 3.17: EDX spectrum of purified Fe-SiO_2 CNTs

(iii) BET analysis

The surface area of carbon nanotubes that contained SiO_2 is less than that of CNTs produced over the unpromoted catalyst. The Figure 18 shows that the surface area decreased for the carbon nanotubes produced over the promoted catalyst. The specific surface area of the product was found to be 85 m^2/g, while CNTs produced over the promoted iron catalyst was 55 m^2/g with pore volume of 0.19 cm^2/g.

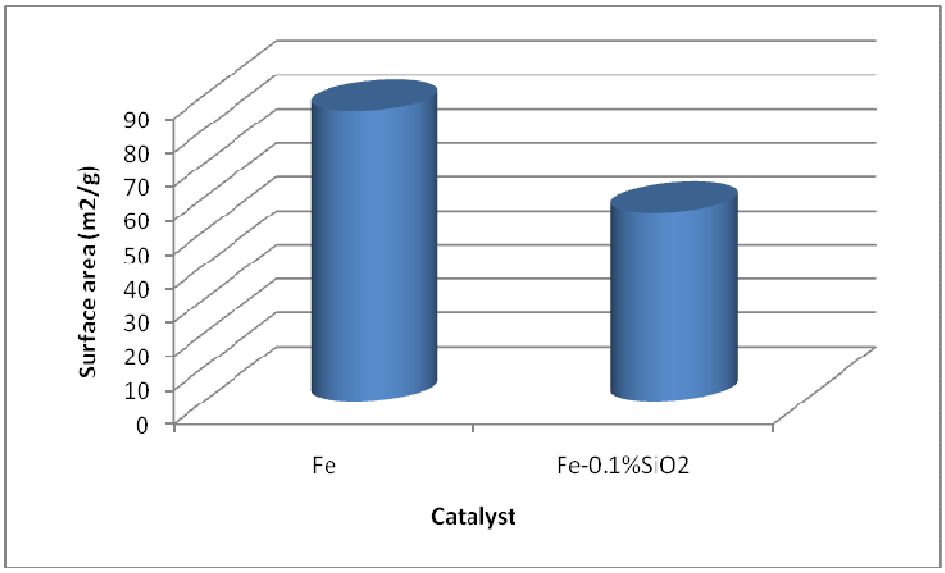


Figure 3.18: Surface area for Fe and Fe-SiO_2 CNTs

(iv) Raman analysis

The D and G band intensities and positions were recorded (Figure 19 and Table 4). The I_D/I_G value is equal to 1.3 and 1.1 respectively which suggests a greater degree of defects in CNTs structure produced over Fe/SiO_2 catalyst.

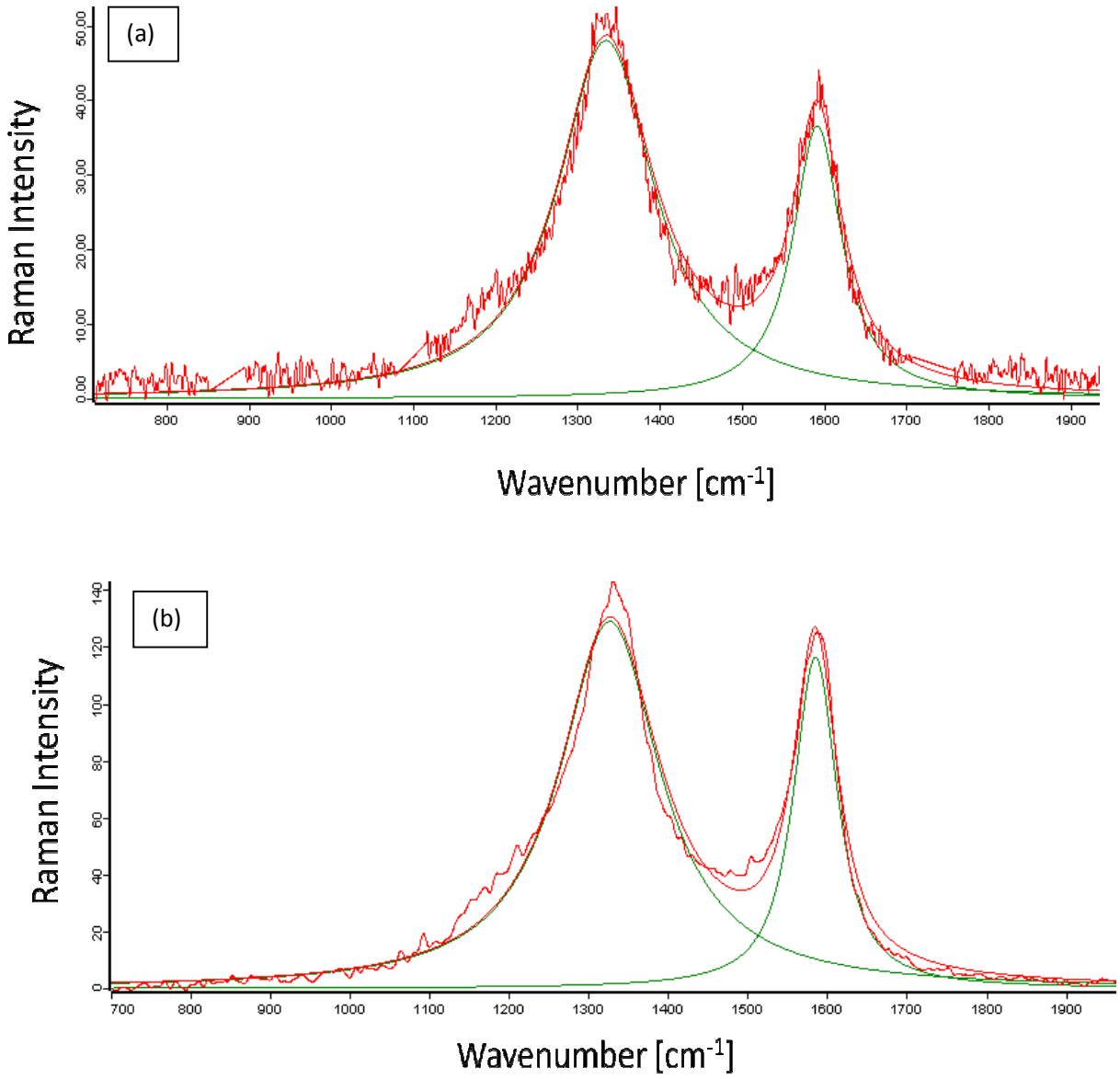


Figure 3.19: Raman spectra of (a) 10% Fe (b) 10%Fe-0.1%SiO_2 samples

Table 3.4*: Peak positions of the purified samples and the intensity ratio of the bands*

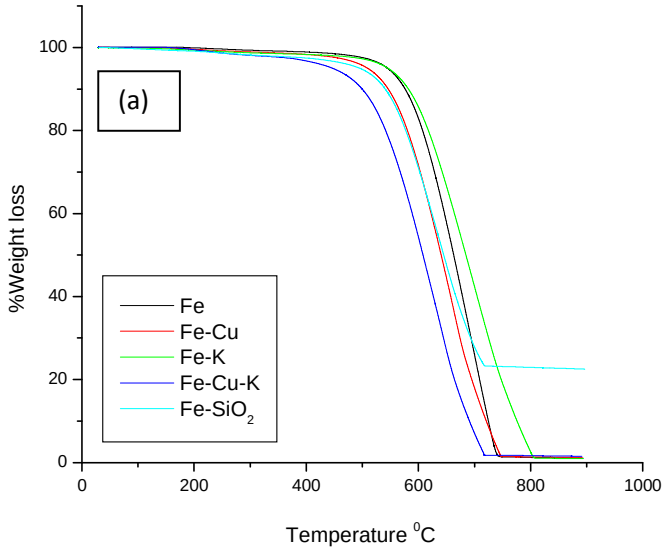
Sample name	Position	Intensity	Bandwidth	Integral	Line shape[a]	I_D/I_G	RMS[b]
Fe	1334.83	48.158	142.49	10778	100%Lorentz+Gauss	1.3	2.17
	1592.27	36.656	72.50	4174	100%Lorentz+Gauss		
Fe/SiO_2	1326.83	129.291	153.53	31181	100%Lorentz+Gauss	1.1	4.43
	1585.51	116.839	66.51	11758	89%Lorentz+Gauss		

3.1.5 Thermogravimetric Analysis (TGA) of CNTs performed in air

It is well known that the TGA technique can be used to determine the purity and gives information on the degree of crystallinity of CNTs. The carbon content of different carbonaceous materials can be associated with the weight loss when carbon is oxidized in air [18]. Purified unpromoted Fe and promoted Fe with Cu, K and Cu/K samples show an approximately 98% mass loss when heated in air (Figure 20 and Table 5). SiO_2 promoted Fe shows about 75% mass loss at a temperature greater than 400^{o}C. This may be due to the incomplete extraction of SiO_2 by HF of the CNTs produced using Fe promoted with SiO_2. It is to be noted that the unpurified samples showed a higher non-carbon residue, due to the presence of catalyst, promoter and support. These impurities can be removed by a dilute acid wash. The 2% residue left in the CNT sample may be attributed to Fe oxide [18]. The TGA profile of all the purified CNTs clearly shows that CNTs commence oxidation at a relatively low temperature (400 ^{o}C). The presence of the lower oxidation temperature implies that lattice defects trigger and accelerate the oxidation process, which is supported by the presence of greater a slope in the TGA curves [19].

The effect of the promoters on the carbon combustion can be evaluated from the TGA curves (Figure 20b). The peak positions can be correlated with the ease/difficulty of the oxidation process. The addition of promoters generally lowered the oxidation temperature. This would suggest more defects in the carbon structure were produced in the presence of the promoters

(Table 5). Addition of K raised the oxidation temperature; this agrees with Raman data of Fe/K samples. Interestingly, the addition of both Cu and K gave the lowest CNT oxidation temperature, suggesting the most defective CNTs had been produced by this promoter combination. An interesting feature relating to the derivative curves is that all the promoted samples show two maxima. The second maxima occur on the higher temperature side of the curve. This would suggest a more crystalline carbon has been produced in the sample. Again, the implication from the data is that a more heterogeneous carbon material has been produced in the presence of all the promoters.



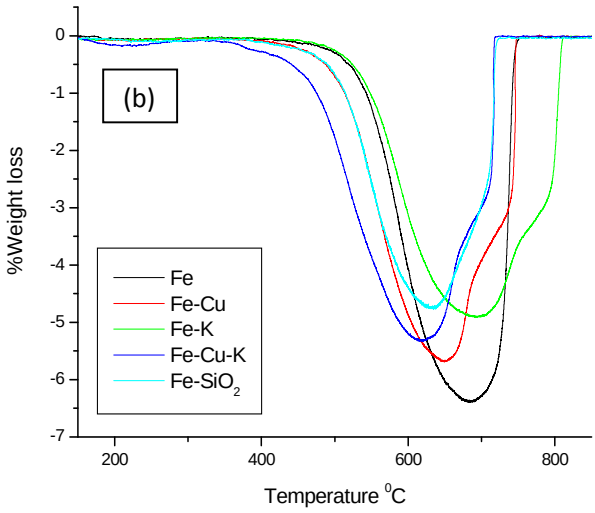


Figure 3.20: TGA (a) Fe, Fe/Cu, Fe/K, Fe/Cu/K, Fe/SiO_2 profiles and (b) Fe, Fe/Cu, Fe/K, Fe/Cu/K, Fe/SiO_2 derivative curves of purified CNTs.

Table 3.5: ***Data from the derivative curves.***

Catalyst	Temperature (^{0}C)	Weight loss (%)
10%Fe	680	98
10%Fe-0.6%Cu	650	98
10%Fe-0.4%K	690	98
10%Fe-0.4%k-0.6Cu	620	98
10%Fe-SiO_2	630	75

3.1.6 Effect of temperature and promoter loading on the Fe catalyst.

Prior to the results given in sections 3.1.1 to 3.1.4 a series of reactions were performed in which both reaction temperature as well as the promoter loading were varied. The results of these extensive studies are summarized in Table 3.6. This set of data was used to generate samples for further characterization.

Some generalizations that derive from the study are:

1. As the temperature increased from 600 to 700°C the yield of product decreased over the Fe catalyst and went through a minimum at 650°C for the Fe/K (0.4%) and Fe/Cu (0.6%) catalysts. In every instance the higher yields were obtained at 600°C. For these reasons 600°C was chosen as the reaction temperature for the study.
2. An increase in K loading from 0.4 to 0.6 to 1.0% revealed a decrease in CNT yield with K loading.
3. For the Cu promoter, a 0.6% loading gave a higher product yield than that produced at 0.4 and 1.0% Cu loadings.

The above data is summarized in Figures 3.21 and 3.22.

Table 3.6: Properties of purified MWCNTs produced as a function of promoter loading

Temperature (°C)	**Catalyst composition (Wt. %)**	**MWCNTs produced**		
		Yield (mass/g)	BET surface area (m^2/g)	Pore Volume (cm^3/g)
600	10Fe/$CaCO_3$	2.27	85.48	0.190
	10Fe-	3.46	47.37	0.141

	0.4K/$CaCO_3$			
	10Fe-0.6K/$CaCO_3$	1.70	56.10	0.234
	10Fe-1K/$CaCO_3$	1.53	54.56	0.223
	10Fe-0.4%Cu/$CaCO_3$	2.91	77.02	0.298
	10Fe-0.6Cu/$CaCO_3$	4.04	100.54	0.225
	10Fe-1Cu/$CaCO_3$	3.38	92.25	0.241
	10Fe-0.4K-0.6Cu/$CaCO_3$	2.98	74.48	0.335
650	10Fe/$CaCO_3$	1.38	30.01	0.164
	10Fe-0.4K/$CaCO_3$	1.46	49.11	0.214
	10Fe-0.6Cu/$CaCO_3$	2.12	59.87	0.241
700	10Fe/$CaCO_3$	0.86	28.63	0.126
	10Fe-0.4K/$CaCO_3$	1.72	78.14	0.201
	10Fe-0.6Cu/$CaCO_3$	3.61	51.29	0.229

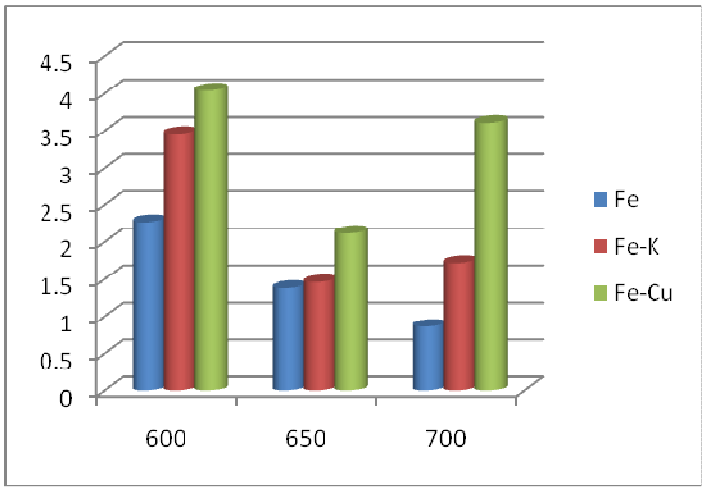


Figure 3.21 : Yield of Fe, Fe-K, Fe-Cu obtained over temperature 600, 650 and 700^{0}C

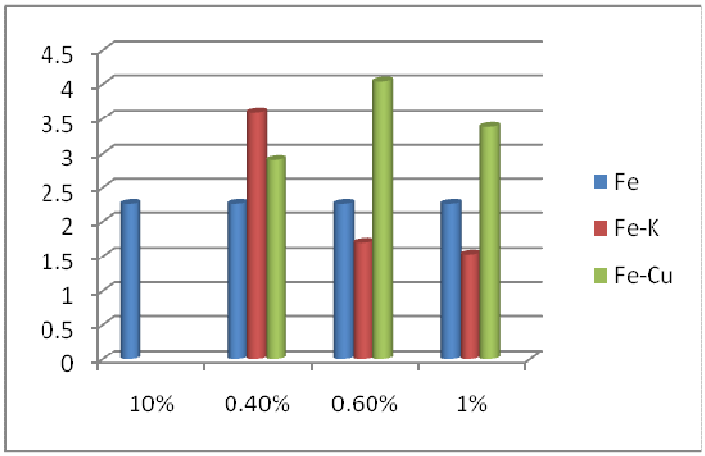


Figure 3.22 : Yield obtained over 10%Fe, 10%Fe-0.4%Cu and K, 10%Fe-0.6%Cu and K, 10%Fe-1%Cu and K catalyst containing various amount of loadings of Cu an K promoters.

3.1.7 Effect of carrier gas on CNT production

The effect of carrier gas on the CNT synthesis reactions was also investigated. Instead of H_2, N_2 was used as an inert carrier gas. Although the flow rates were not equivalent the effect of a reducing gas could be evaluated from the study.

(i) Effect on yield, H_2 is known to aid the Fe reduction process, especially at temperatures greater than 500°C. Thus it would be predicted that the use of N_2 would result in lower CNT yields as less Fe would be in a reduced state and the catalytic behaviour would hence be lowered. Data for a comparative study are given in Tables 8 and 9. As expected the use of H_2 resulted in the unpromoted Fe catalyst producing more carbonaceous products. Surprisingly, addition of K also promoted the formation of more products. The effect of Cu is as predicted. Under N_2 a small effect is seen, under H_2 the effect is dramatic. This is expected from the known behaviour of Cu on the Cu promoted Fe catalyst. Cu aids the Fe reduction process [20].

(ii) Effect on the morphology. The effect on the carbon morphology produced was quite dramatic.

(a) Fe unpromoted catalyst. Fe produced both tubes and spheres when N_2 was used. This is not unexpected as acetylene decomposition in the absence of catalyst is known to produce spheres.

(b) The quality of the CNTs produced under N_2 was found to be excellent compared to those produced under H_2 (Figure 3.23).

Table 3.8: Reaction conditions of the synthesis of CNTs under H_2[a]

Catalyst	Temperature (°C)	Yield (g)
10%Fe	700	0.86
10%Fe-0.6%Cu	700	3.61
10%Fe-0.2%K	700	1.53

[a]Gas flow rate ; Acetylene 100 ml/minute, Hydrogen 100 ml/minute

Mass of catalyst = 0.5 g

Table 3.9: Reaction conditions of the synthesis of CNTs under N_2[a]

Catalyst	Temperature (°C)	Yield (g)
10%Fe	700	0.42
10%Fe-0.6%Cu	700	1.30
10%Fe-0.2%K	700	0.56

[a]Gas flow rate; Acetylene 90 ml/minute, Nitrogen 240 ml/minute

Mass of catalyst = 0.5 g

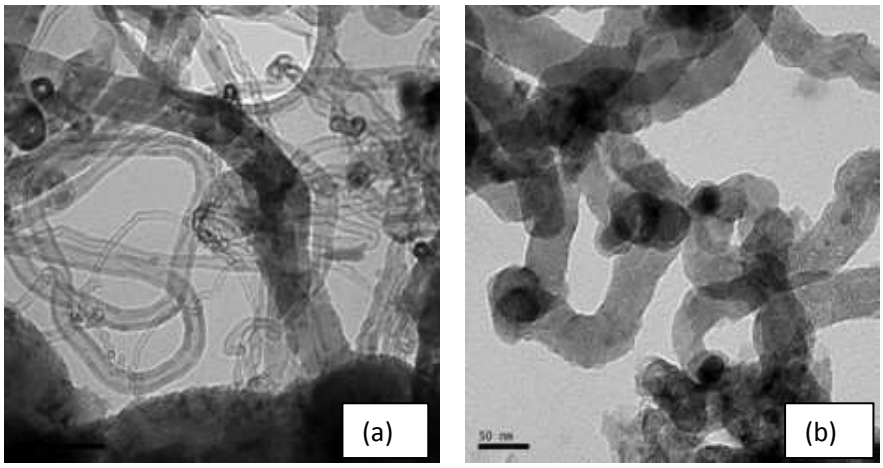


Figure 3.23: TEM images of unpurified CNTs (a) 10%Fe (N_2) (b) 10%Fe (H_2)

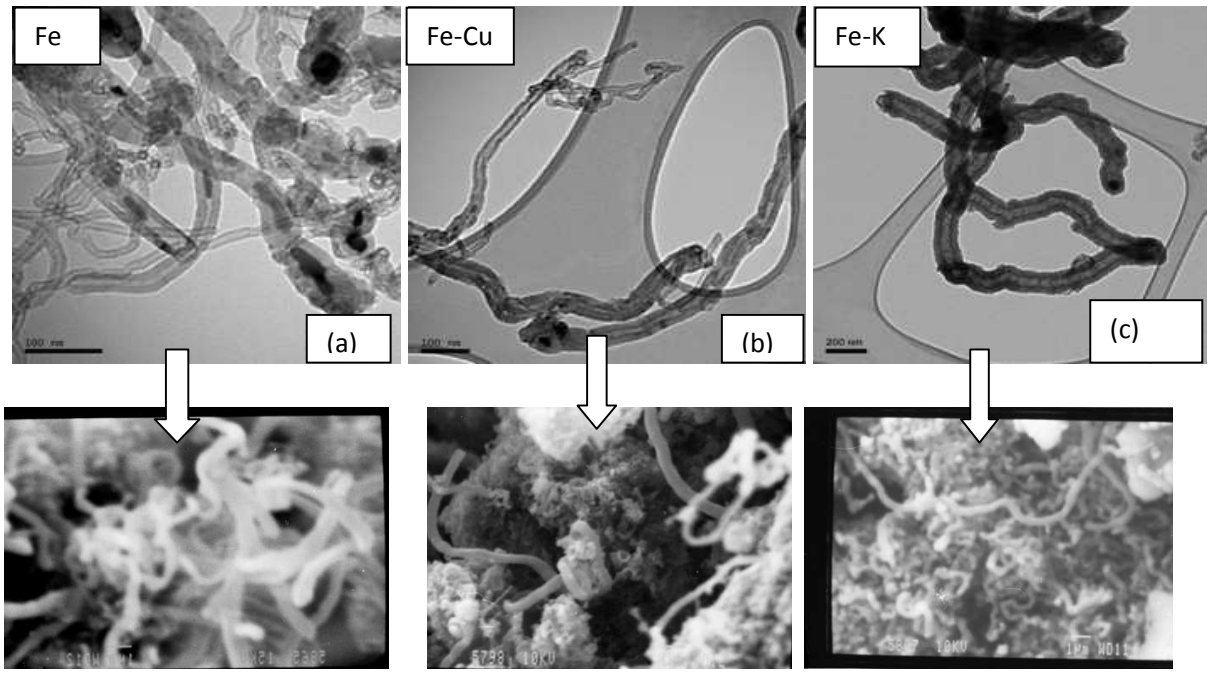


Figure 3.24: TEM and SEM images of unpurified CNTs (a) 10%Fe (b) Fe-0.6%Cu (c) Fe-0.2%K at 700^{0}C under N_2

TEM and SEM results showing the effects of Cu and K promoters under N_2 are shown in Figure 24. TEM analysis revealed that carbon nanotubes have dark spots inside the tubes which are Fe particles. The Fe -K shows a rough surface for the CNTs. From SEM images it can be seen that the carbon nanotubes are long and the wall surface is clean. Addition of a small amount of Cu (0.6%) to 10% Fe increased the yield of the CNTs from 0.42 g to 0.56 g and K (0.2%) increased the yield to 1.30 g.

The TGA profile for unpurified Fe-CNTs differs from other TGA profiles at the start of oxidation, i.e. about 3% weight increase. This observable fact is due to the O_2 diffusion through lattice defects to react with encapsulated Fe, thus forming Fe_2O_3, and the residual weight 35% is also oxide [21]. Unpurified material for Fe-Cu, Fe-K and Fe showed that about 20%, 65% and 35% respectively of the impurities remain behind. The purified material for Fe-Cu, Fe-K and Fe showed that about 10%, 9%, 23% respectively of the impurities remain behind after performing TGA up to 900°C. The residual are attributed to the iron oxide and other impurities. TGA results that showed purified CNTs by 30% HNO_3 had the highest weight loss (%) due to amorphous carbon that has been removed.

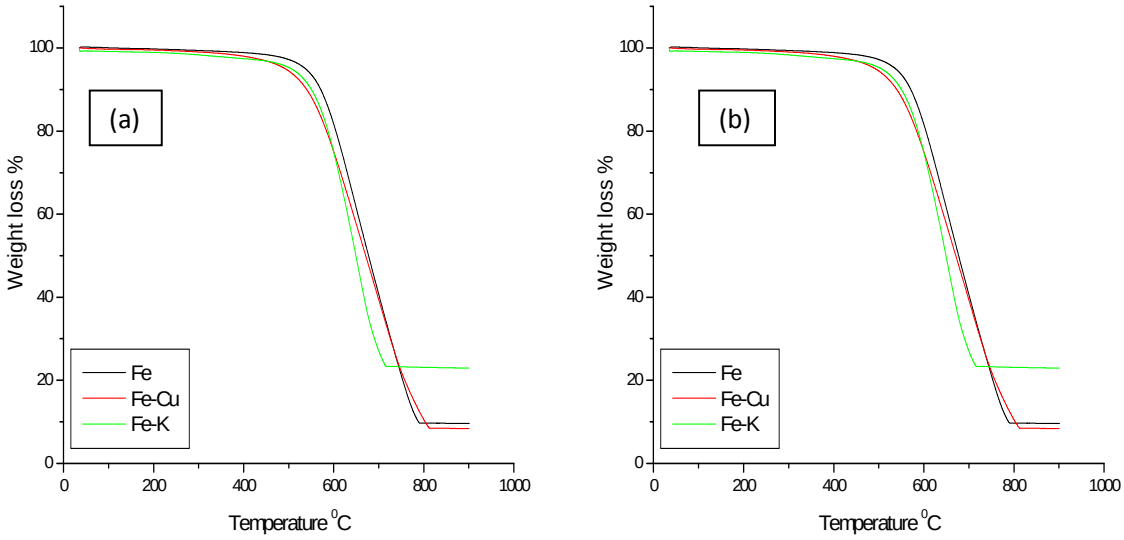


Figure 3.25: TGA profile of (a) unpurified and (b) purified CNTs

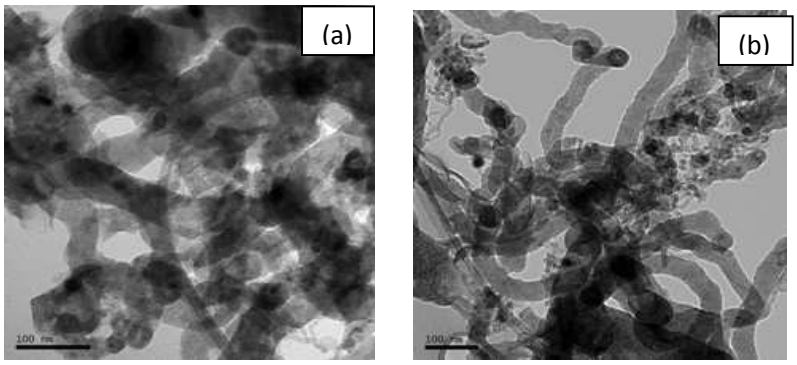


Figure 3.26: TEM images of (a) unpurified and (b) purified Fe/CNTs

4 Conclusion

CNTs were successfully synthesized by CVD process using unpromoted and promoted catalysts with Cu, K, and Cu-K promoters. The promoted catalysts improved the catalytic activity of the Fe for CVD synthesis of CNTs. The yield of the carbon material produced from promoted catalyst increased. Addition of small amount of Cu, K and SiO_2 to the Fe catalyst increased the yield. The average diameter of the promoted materials was also increased compared to the unpromoted catalyst. Cu promoted catalyst affects the morphology of the CNTs produced.

The temperature 600°C was chosen as the reaction temperature in this study due to the high yield obtained at this temperature. As the temperature increased the yield of the product decreased over these catalysts. The effect of carrier gas was also investigated. The quality of the CNTs produced under N_2 was found to be the best compared to H_2 but the use of N_2 resulted in a lower CNT yields.

TGA results revealed that the synthesized under H_2 contain a small amount of inorganic residue compared to the catalysts synthesized under N_2 where the inorganic residue for Fe is 10%, Fe-Cu is 9% and Fe-K is 23%. All of these materials were purified by 30% HNO_3. This shows that there is a significant amount of Fe oxide left from the CNTs synthesized under N_2 while the CNTs synthesized under H_2 do not show a substantial amount of impurities.

5 References

[1] Coquay P, Peigney A, De Grave E, Flahaut E, Vandenberghe R.E, and Laurent C, J. Phys. Chem. B **109** (2005) 17813.

[2] Pirard S, Douven S, Bossuot C, Heyen G and Pirard J, Carbon **45** (2007) 1167.

[3] Singh B, Cho S, Bartwal K, Hoa N and Ryu H, Solid State Commun. **144** (2007) 498.

[4] Balogh Z, Halasi G, Korbély B and Hernadi K, Appl. Catal. A: Gen. **344** (2008) 191.

[5] Tsoufis T, Xidas P, Jankovic L, Gournis D, Saranti A, Bakas T and Karakassides M, Diam. Relat. Mater. **16** (2007) 155.

[6] Hornyak G.L, Dillon A.C , Parilla P.A , Schneider J.J, Czap N, Jones K.M , Fasoon F.S , Mason A and Heben M.J, Nanostruct. Mater. **12** (1999) 83.

[7] Zhao G, Zhanga C, Qina S, Xianga H, Li Y, J. Mol. Catal. A: Chemical **286** (2008) 137.

[8] Bahome C.M, Jewell L.L, Hildebrandt, Glasser D, Coville N.J, Appl. Catal. A: General **287** (2005) 60.

[9] Van Steen E, Prinsloo F.F, Catal. Today **71** (2002) 327.

[10] Hayakawa H, Hisanori T, Kaoru F, Appl. Catal. A: General **310** (2006) 24.

[11] Moodley P, Loos J, Niemantsverdriet J.W, Thune P.C, Carbon **47** (2009) 2002.

[12] Kim J.S.C, The role of hydrogen in the growth of carbon nanotubes: A study of the catalyst state and morphology, BSc report, Massachuselts institute of technology, 2006.

[13] Mhlanga S.D, Synthesis and study of carbon nanotubes and spheres, PhD Thesis, University of Witwatersrand, Johannesburg, 2009.

[14] Qi X, Zhong W, Deng Y, Au C, Du Y, J. Phys. Chem. C **113** (2009) 15934.

[15] Kim S, Kim K, Ahn H, Cho K, J. Alloy Comp. **449** (2008) 27.

[16] Hiura H, Ebbesen T.W, Tanigaki K, Takahashi H, Chem. Phys. Lett. **202** (1993) 509.

[17] Cheng J.P, Zhang X.B, Liu F.Tu J.P, Lu H.M, Sun Y.L, Chen F , Mater. Chem. Phys. **87** (2004) 241.

[18] Chen M; Hung-Wei Y, Jhih-Hong C, Horng-Show K, Diam. Relat. Mater. **16** (2007) 1110.

[19] Mei-Hua X, Xiao-Si Q, Wei Z, Xiao-Juan, Yu D, Chaktong A, Chang Q, Zai-Xing Y, You-Wei D, Chin. Phys. Lett. **26** (2009) 116103.

[20] O'Brein R.J, Davis B.H, Catal. Lett. **94** (2004) 1.

[21] Watts P.C.P, Ponnampalam D.R, Hsu W.K, Barnes A, Chambers B, Chem. Phys. Lett. **378** (2003) 609.

Chapter 4
FT Synthesis
Results and Discussion

4.1 Introduction

This chapter represents a preliminary study of the use of the new CNTs (produced in Chapter 3) in Fischer-Tropsch (FT) synthesis. Most of the time spent on the study was devoted to the synthesis and characterization of the CNTs. Thus the main focus of this chapter was on obtaining the first data on the use of the CNTs in a catalytic reaction. The differently produced CNTs should have different amounts of residual catalyst and promoters left on the surface (Cu, Fe, and K). In this study the CNTs investigated were those produced from Fe, Fe-Cu, Fe-K, Fe-Cu-K and Fe-SiO_2 all supported on $CaCO_3$. The other materials will only be investigated in studies by other group members.

The FT synthesis is in principle a carbon chain building reaction, where CH_2 groups are attached to a growing carbon chain. The two main characteristics of Fischer-Tropsch synthesis (FTS) are the production of a wide range of hydrocarbon products (olefins, paraffins, and oxygenated products) and the release of a large amount of heat from the highly exothermic reaction. The FT process produces different olefins and paraffins with different lengths. The process is a chain-building reaction, in which the chain either gains length by incorporating another carbon atom, or terminates and desorbs the catalyst as either paraffin or an olefin. This is graphically shown in Figure 1. Figure 1 shows that there are two reaction possibilities; either the growing chain terminates to form a paraffin (right side) or an olefin (arrow to the left), or the chain continues to grow further by addition of a CH_2 unit which is generated by the absorption of CO and H_2 [1].

In this chapter the effect of promoters on the catalytic activity of a Fe/CNT catalyst is described. Studies by other workers have also been reported on the FT reaction using Fe/CNT catalyst and

also Fe/AlO_3 catalyst and this study will be compared with the other studies. The ranges of promoters used in other studies are shown in Table 1.

Table 4.1*: Different levels of promoters and supports*

Promoters	Promoter loading (%)	Support	Reference
Cu, K	0.6, 0.4	CNTs	[2]
Cu, K	1.2, 4.7	CNTs	[3]
Cu	1.00	Al_2O_3	[4]
K	3.00	Al_2O_3	[5]

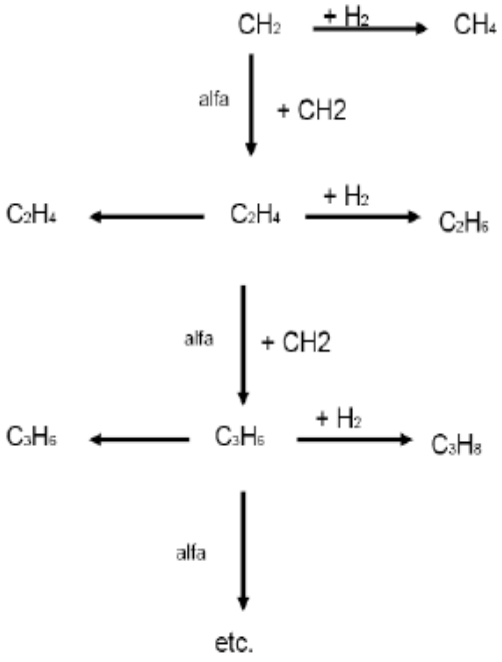


Figure 4.1: Chain growth and termination [1].

4.1.1 Catalyst characterization

Prior to the FT reaction all the catalysts, either unpromoted or promoted with Cu and K (see section 2.2.2 for details) were characterized using different techniques as described below (Table 2, 3, 4). Each catalyst was tested for performance in the FT reaction. Selectivities and conversions for these catalysts are also shown below (Table 5 and Figure 4).

It is well known that the promotion of iron by potassium has a significant effect on the FT performance of catalysts, since K is assumed to donate electrons to the vacant d orbital of the transition metal. Potassium suppresses the production of methane and improves the effective hydrocarbon selectivity [5]. Much literature has been reported on the interaction between potassium and structural promoters in Fe based FT catalysts. The reports also revealed that there is a K-support interaction in catalysts, which decreases the promotional effect of K on FT activity and selectivity [6]. It has been reported that the addition of copper enhances the rate of reduction of Fe catalysts for FT synthesis [7]. The Cu promotion enhances the activity of supported Fe catalysts but does not have an effect on FT product selectivity [4]. If the promoters (Cu, K) are used they have an effect on both the activity and selectivity of iron catalysts.

Table 4.2: ***Metal content of various catalysts determined by ICPOES*** [a]

Catalyst	%Fe	%Cu	%K
10%Fe/CNTs	10.4	0	0
10%Fe- 0.6%Cu/CNTs	9.6	0.65	0
10%Fe-0.4%K/CNTs	10.5	0	0.38

[a]ICPOES = Inductive Coupled Plasma-Optical Emission Spectroscopy

The results obtained in Table 1 revealed the exact amount of the metal ratios added in the catalyst that are close to the predicted values from the catalyst preparation.

Table 4.3: ***Surface area analysis of catalyst determined by BET***

Catalyst	Surface area (m^3/g)	Pore volume (cm^3)	Pore size (nm)
10%Fe/CNTs	62	0.162	10.4
10%Fe-0.6%Cu/CNTs	88	0.138	6.2
10%Fe-0.4%K/CNTs	52	0.148	11.3

Table 2 shows the BET data of the unpromoted and promoted Fe/CNTs used. It is seen that the addition of Cu increases the surface area of the unpromoted catalyst while addition of a K promoter decreases the surface area when added to the catalyst precursor. These promoters increase the pore size of the catalyst precursor.

Bahome et al [8] studied the effect of these promoters (Cu, K) and they discovered that addition of the Fe and promoters to the CNTs resulted in a reduction of the surface area. Duvenhage et al [9] reported an increase of the surface area on K promotion but this was on a TiO_2 support. Also it was mentioned that very low levels of K increase the effective surface area of catalysts and as a consequence the activity.

TEM analysis performed on a range of catalysts (Figure 1) revealed that the catalyst particles grow at the tip of the carbon nanotubes. Many of the carbon nanotubes are open at the end, and Fe metal particles are observed on the surface of CNTs and do not affect the morphology of the CNTs.

.

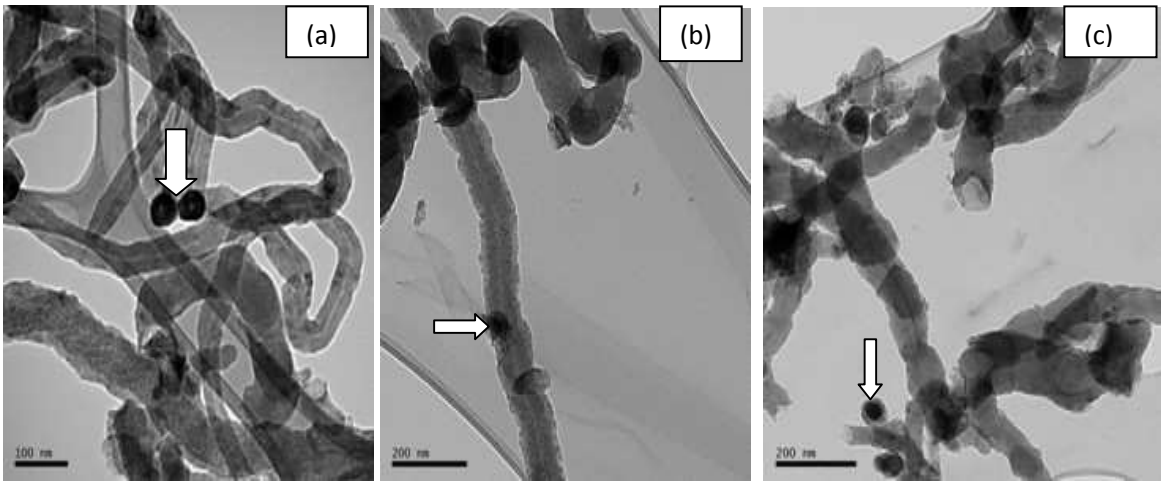


Figure 4.2: TEM image (a) 10%Fe/CNTs (b)10%Fe-0.6%Cu/CNTs and (c)10% Fe-0.4% K

4.1.2. Reduction behavior of the catalysts

A TPR study was carried out on the unpromoted Fe catalyst and the Cu, K promoted catalyst containing different loadings of promoter. Figure 2 shows the TPR profiles of 10%Fe/CNTs, 10%Fe-0.6%Cu/CNTs, and 10% Fe-0.4%K/CNTs. The reduction of iron oxides takes place in consecutive steps: $Fe_2O_3 \rightarrow Fe_3O_4 \rightarrow FeO \rightarrow Fe$. The first peak can be asigned to the reduction of Fe_2O_3 to Fe_3O_4. The peak observed (or shoulder) observed at ~ 350ºC is associated with the reaction Fe_2O_3- Fe_3O_4. The peak at 450ºC is associated with reduction of Fe_3O_4 to FeO. The peak observed at 500-600ºC can be related to the reduction of FeO to metallic Fe. At temperatures higher than 600ºC gasification of the CNTs occurs [10]. Cu is able to lower the reduction temperature of Fe hence providing more active sites for catalyst at the lowest temperature. The reduction peak at 225ºC is associated with a transformation of both CuO → Cu and $Fe_2O_3 \rightarrow Fe_3O_4$ [2]. Table 3 shows the reduction temperatures for all the catalysts.

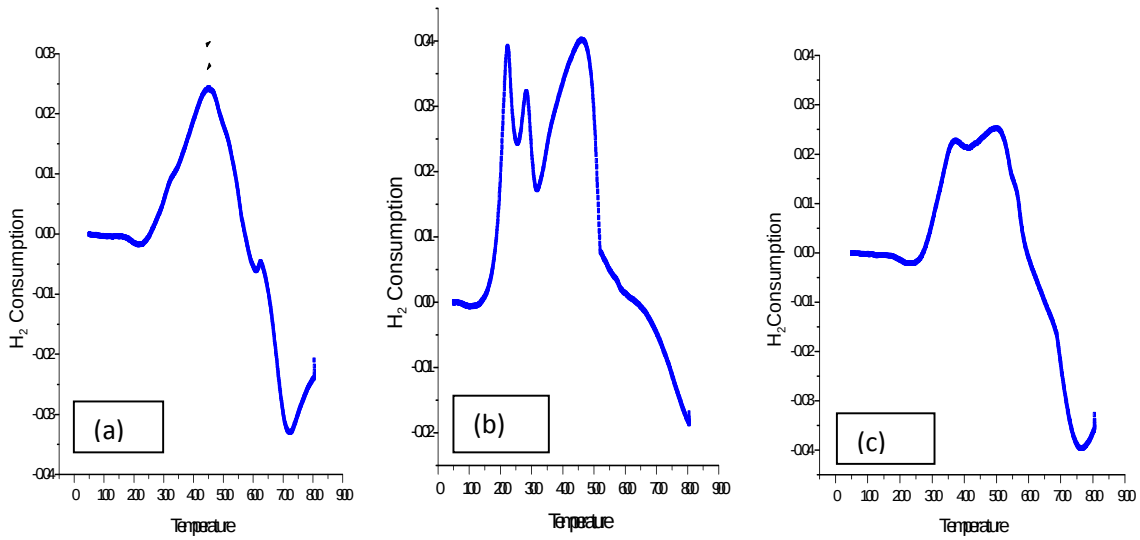


Figure 4.3: TPR profiles (a) 10%Fe/CNTs, (b) 10%Fe-0.6%Cu/CNTs (c) 10%Fe-0.4%K.

Table 4.4*: Fe peak positions of the catalyst obtained from a TPR profile.*

Catalyst	Peak 1	Peak 2	Peak 3
Fe	330°C	450°C	630°C
Fe-Cu	290°C	480°C	
Fe-K	375°C	525°C	560°C

[a]Peak at 225°C due to CuO → Cu reduction and possible some Fe reduction.

[b]Reduction temperature (°C) based on H_2-TPR analysis.

Bukur and Sivaraj suggested that only a small portion of the iron oxide is reduced to metallic iron during the first reduction process, with most of the Fe_3O_4 being reduced at a higher temperature (second peak) [11].This study shows that all the peaks in the Cu promoted catalyst were shifted to lower temperature when compared with the unpromoted catalyst and the K promoted catalyst shows a shift of peaks to higher temperature. Pansanga et al [4] reported that the Cu- modified Fe/Al_2O_3 catalyst was similar to Fe/Al_2O_3 with only a single reduction peak being observed.

4.1.3 Catalyst tests, data analysis and calculations

Catalyst tests were carried out in a fixed bed reactor. The catalyst (0.5 g) was reduced in a flow of hydrogen (2 bar, 623 K) and then cooled to room temperature before switching the gas stream to a H_2/CO mixture at 8 bar, 548 K, and H_2/CO ratio of 1:2. The catalytic results were recorded at steady state after stabilization. The CO, H_2, CO_2, and CH_4 products were analyzed using TCD. The gas products were separated by the capillary column and then detected using FID. Liquid products and wax were collected in a cold trap and a hot trap, respectively.

The calculations that were used in this study are similar to those described by Duvenhage et al [13]. % CO conversion was calculated as follows:

$$CO\ (\%) = \left[\frac{CO_{in} - CO_{out}}{CO_{in}} \frac{N2\ in}{N2\ out}\right] * 100$$

The product selectivity for hydrocarbons was calculated as follows:

$$S_i = \left[\frac{mass\ components}{\Sigma xi}\right] * 100$$

The FTS rate (r_{FTS}) and water gas shift rate (r_{WGS}) were calculated from the values obtained in the experiment.

$r_{WGS} = r_{CO2}$

$r_{FTS} = r_{CO} - r_{CO2}$

Where r_{CO} is the rate of carbon monoxide conversion and r_{CO2} is the rate of carbon dioxide formation.

Olefins and paraffins ratio = mass olefin/ mass total hydrocarbon.

$\log (Wn/n) = n \log (\alpha) + \log ((1- \alpha)/\alpha)^2$

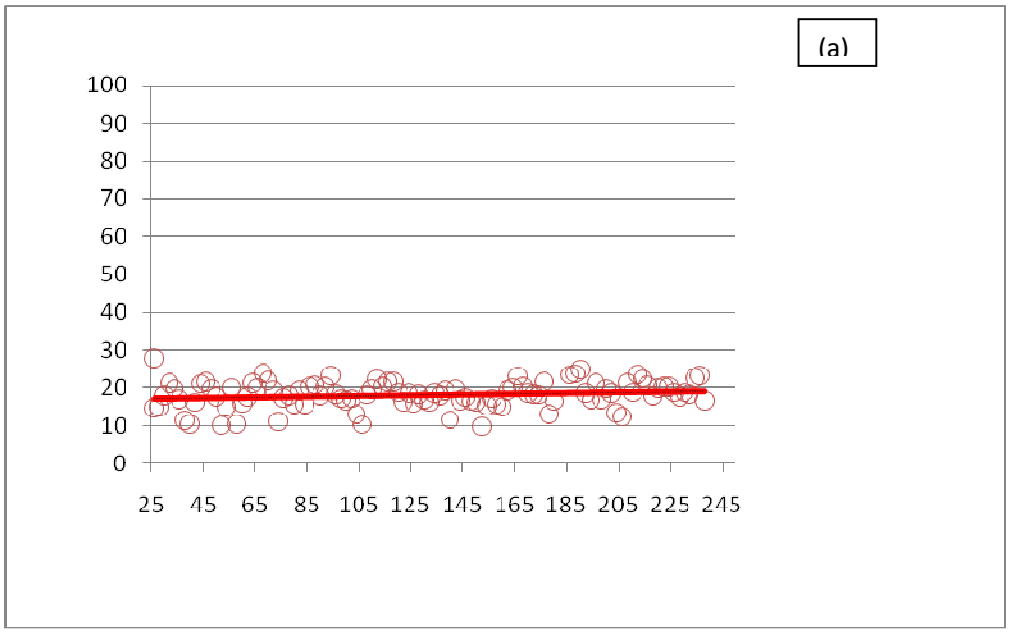
This equation is used to determine α value from experimental data. A plot of log (Wn/n) versus carbon number (n) is linear and the chain growth probability is obtained from its slope as log (α) or from the intercept as $\log ((1-\alpha)/\alpha)^2$ at n = 1.

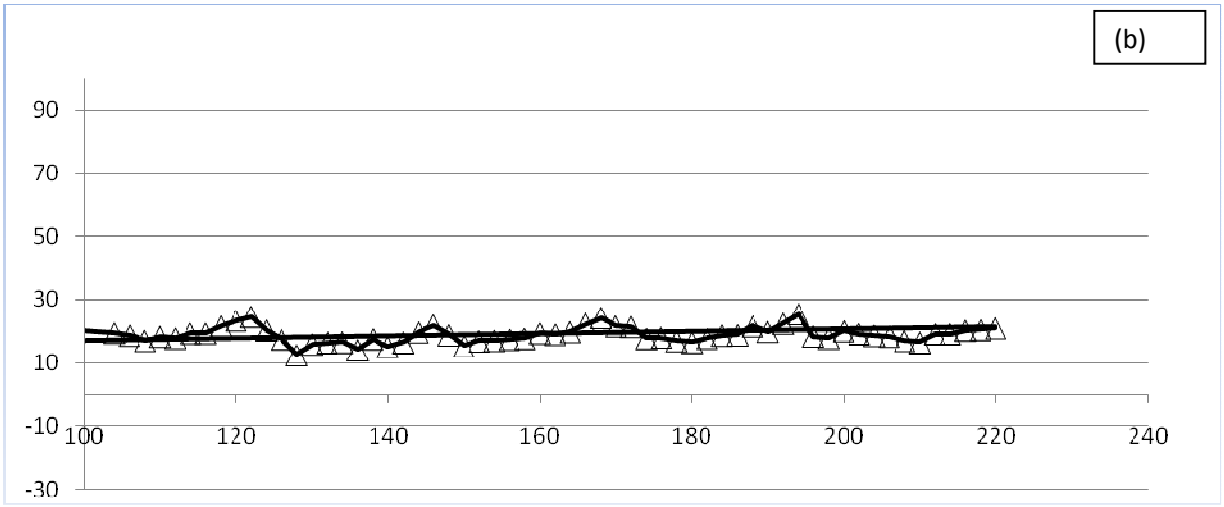
4.1.4 Catalytic performance

The performances of the catalysts were measured in a fixed-bed reactor. All the reactions were performed under a standard set of conditions (T = 275°C, P = 8 bar, Flow rate = 20 ml/min. H_2: CO = 2). CO hydrogenation studies were performed on the unpromoted iron catalyst and the iron catalyst promoted with Cu, K. Figure 4.4 shows the CO conversion as a function of time on-stream (TOS). In the case of the Cu promoted catalyst the CO conversion is the same as that observed for unpromoted catalyst (19% and 18%) respectively, The K promoted catalyst gave a similar activity (22%). The addition of K promoter has been reported to increase the CO conversion [5].

Table 4.5*: Activity, CO conversion and Selectivity of iron catalyst.*

Catalysts	Activity (μmol/sec.g)	Conversion (%)	Selectivity	
			C_1	$C_2=/C_2$
Fe	14.8	18	28.17	0.04
Fe-Cu	13.7	19	29.31	0.03
Fe-K	14.7	22	24.11	0.26


(a)
100
90
80
70
60
50
40
30
20
10
0
25 45 65 85 105 125 145 165 185 205 225 245


(b)
90
70
50
30
10
-10
-30
100 120 140 160 180 200 220 240

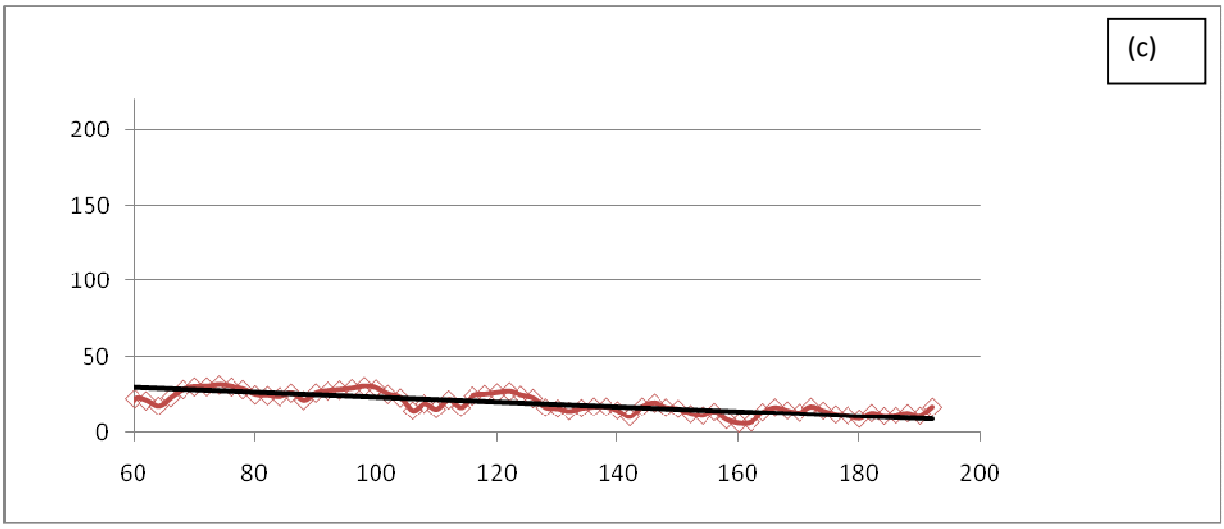


Figure 4.4: CO conversions with time on stream (a) Fe/CNT (b) Fe-Cu/CNT (c) Fe-K/CNT.

4.1.5 Product selectivity

General Comments:

General observations regarding the effect of potassium promotion on iron catalysts for FTS include (a) an increase in the average molecular weight (chain length) of hydrocarbon products (i.e., decrease in production of methane and light gases), (b) an increase in olefin selectivity, (c) an increase in activity for the water gas shift (WGS) reaction, (d) an increase in carbon deposition and catalyst deactivation rate, and (e) an increase in FTS activity at low potassium concentrations, followed by a decrease at higher K levels [13].

Copper has been widely used as one of the promoters for FTS on iron catalysts, particularly in bubble column slurry reactors [14-16]. Its function is to decrease the temperature required for reduction of iron oxides. Kolbel et al. [17] observed an increase in the overall activity at very low levels (ca. 0.1 wt %) of copper promotion, with no further enhancement at higher copper loadings. Wachs et al. [18] reported that product distributions did not change appreciably when

copper is incorporated into an iron catalyst for experiments in a differential fixed bed reactor (CO conversion less than 1%).

Zhao et al [5] reported that K promotion restrains the production of C_1-C_4 hydrocarbons and increases the C_{5+} selectivity. The addition of K promoter can markedly increase the CO conversion. Van Steen et al [3] have reported a decrease in CO conversion over an iron catalyst supported on CNTs and promoted with Cu and K. After reduction all three catalysts had similar metal surface areas. But the activity of these catalysts differed significantly in FT synthesis.

Bahome et al [8] reported that the addition of Cu to a Fe/CNT catalyst resulted in an increase in CO reaction rate, activity and CO_2 production rate. Addition of K to the Fe/CNT showed an increase in olefinity and alpha values and a decrease in CH_4 selectivity. The effect of the K on the olefinity of the C_2 hydrocarbon (0.10 -0.72%) is remarkable.

Duvenhage et al [9] reported that the addition of 0.1%K to Fe:Co:K/TiO_2 increased the specific activity, oxygenation formation and olefinity but at high loading of K the reverse occurred. It appears that the promotion enhances behavior expected for the traditional Fe catalyst.

Effects observed in this study:

The product selectivity of the catalysts (CH_4, C_2-C_4, C_{5+} and CO_2) after 225 h on stream is given in Table 6. The data show that the CH_4 selectivity of the Fe/CNTs catalyst (28.17%) is higher than that of Fe-Cu/CNT catalyst (29.31%) and lower than Fe-K/CNT (24.11%), The C_2-C_4 fraction obtained from the Fe catalyst (54.64%) is lower than that obtained from the Fe-Cu catalyst (56.30%) and higher than Fe-K catalyst (50.88%). The CO_2 selectivities of the Fe, Fe-Cu and Fe-K catalysts were formed to be 1.72, 1.47, and 1.38 % respectively. The alpha values of these catalysts are ranging between 0.45 and 0.65.

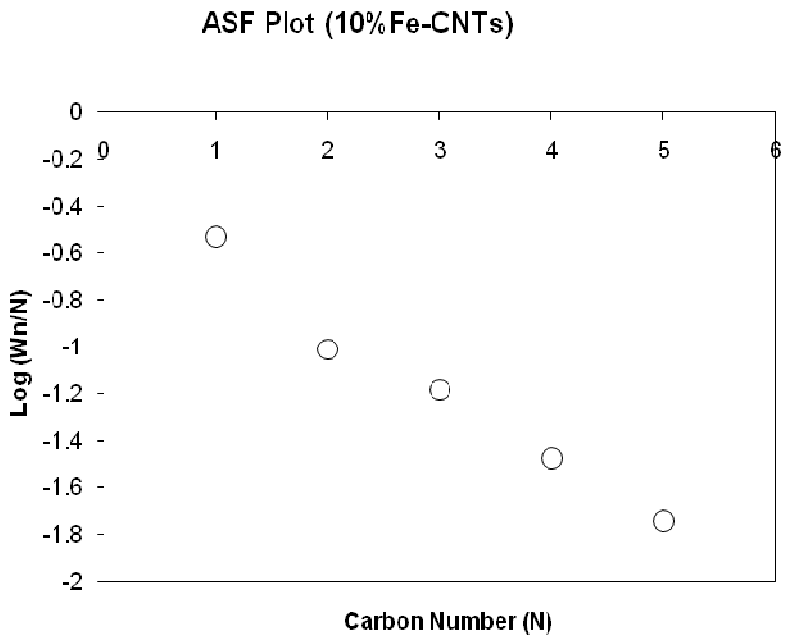
Table 4.6*: Activity and selectivity of iron catalyst in FTS*

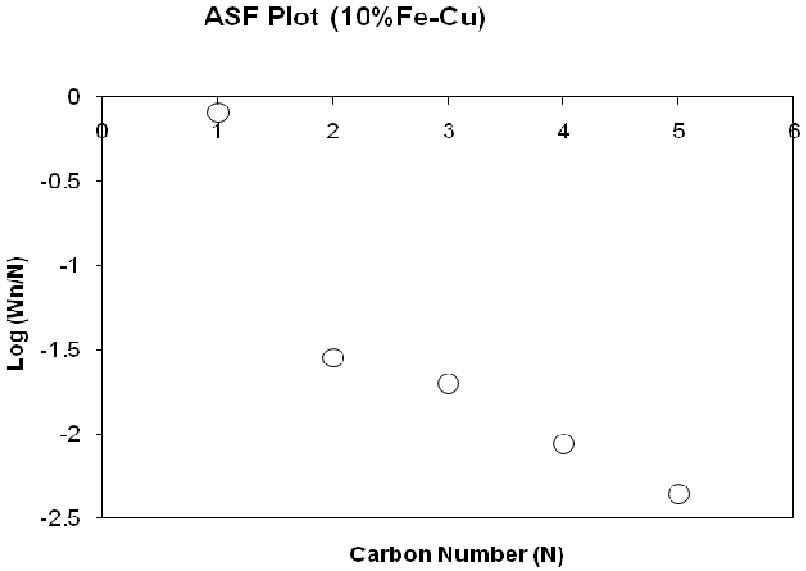
Catalyst	Fe	Fe-Cu	Fe-K
CO rate[a]	7.69E-07	7.56E-07	7.91E-07
CO_2 rate (WGS)	1.07E-07	9.16E-07	8.6E-08
FTS rate	6.62E-07	6.64E-07	7.05E-07
Activity (μmol/sec.g)	15.38	14.26	15.22
Alpha (α)	0.51	0.45	0.65
Selectivity (%)			
C_1	28.17	29.31	24.11
C_2-C_4	54.64	56.30	50.88
C_{5+}	17.18	14.38	25.01
$C_2=/(C_2+C_2=)$[b]	0.04	0.03	0.26
CO_2	1.72	1.47	1.38

Data consist of ± 5% experimental errors.

[a]Rate (mol/s)

[b]Olefin to total C_2 hydrocarbon weight ratio


ASF Plot (10%Fe-CNTs)
Log (Wn/N)
Carbon Number (N)
0
-0.2
-0.4
-0.6
-0.8
-1
-1.2
-1.4
-1.6
-1.8
-2
0
1
2
3
4
5
6


ASF Plot (10%Fe-Cu)
Log (Wn/N)
Carbon Number (N)
0
-0.5
-1
-1.5
-2
-2.5
0
1
2
3
4
5
6

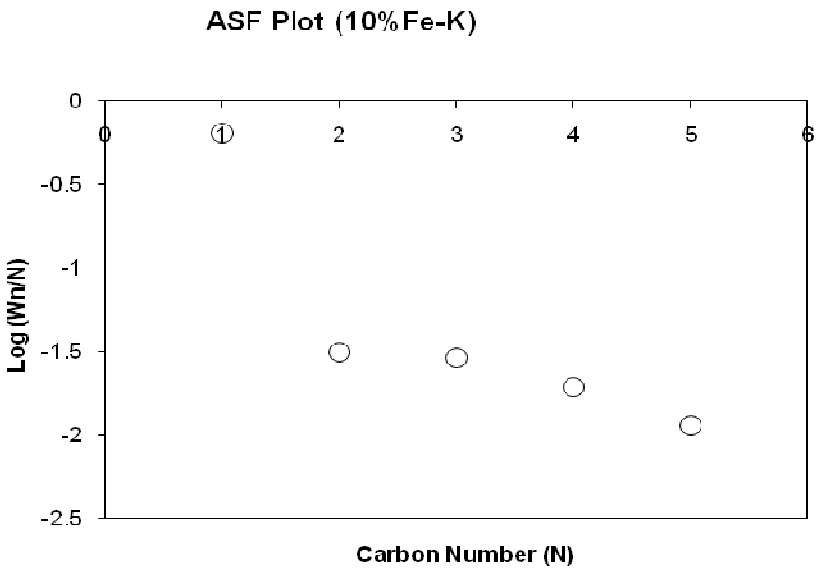


Figure 4.5: Anderson–Schulz–Flory (ASF) Carbon number distribution of hydrocarbons formed over unpromoted Fe and Cu, K promoted iron catalyst [13].

4.8 Conclusions

The results of this research in agreement with the work of Zhao et al. [5] where K enhances the production of olefins and increases the CO conversion. The potassium promoted catalyst has a higher CO rate than that of unpromoted Fe. The results also agree with the findings of Bahome et al. [8] in which K addition enhanced olefinity and the alpha values. The effect of K on the olefinity of the C_2 hydrocarbon in Table 4.5 is 0.04 to 0.26. An increase in FTS activity is also observed on K promoted catalyst. Copper decreases the reduction temperature of iron oxides as shown by TPR studies. Copper promoted catalysts show a high selectivity to methane and a decrease in the C_{5+} and C_2 olefins as well as an increase in the FTS rate.

4.9 References

[1] http://www.zero.no/fischer-tropsch reactor fed by syngas (accessed on 18 January 2010).

[2] Bahome M.C, Jewel L.L, Padayachy K, Hildebrandt D, Glasser D, Datye A, Coville N.J. Appl. Catal. A: Gen.**328** (2007) 243.

[3] Van Steen E, Prinsloo F.F, Catal. Today **71**(2002) 327.

[4] Pansanga K, Lohitharn N, Chien A.CY, Lotero E, Panpranot J, Praserthdam P, Goodwin Jr J.M. Appl.Catal. A: General **332** (2007) 130.

[5] Zhao G, Zhang C, Qin S, Xiang H , Li Y, J. Mol. Catal. **286** (2008) 137.

[6] Yang Y, Xiang H, Xu Y, Bai L, Li Y , Appl. Catal. A: Gen. **266** (2004) 181

[7] Dry M.E , in: J.R. Anderson, M. Boudart (Eds), Catal.Sci. and Technol. **1** (1981) 159

[8] Bahome M.C, Jewel L.L, Hildebrandt D, Glasser D, Datye A, Coville N.J. Appl. Catal. A: Gen.**287** (2005) 60.

[9] Duvenhage D.J and Coville N.J, Catal.Lett. **104** (2005) 3.

[10] Abbaslou R.M.M, Tavassoli A, Soltan J, A.K.Dalai. Appl. Catal. A: Gen. **367** (2009) 47.

[11] Bukur D.B, Sivaraj C, Appl. Catal. A **231** (2002) 201.

[12] Duvenhage D.J, Coville N.J, Appl. Catal. **153** (1997) 43.

[13] Dragomir B. Bukur, D.M, and Patel S. A, Ind. Eng. Chem. Res. **29** (1990) 194.

[14] Kolbel, H.; Ralek, M. Catal. Rev. Sci. Eng. **21** (1980) 225.

[15] Deckwer,W.D; Serpemen, Y.; Ralek, M.; Schmidt, B. Ind. Eng. Chem**.** Process Des. Dev. **21**(1982) 222.

[16] Kuo, J. C. W. Two Stage Process for Conversion of Synthesis Gas to High Quality Transportation Fuels. Final Report DOE Contract DE-AC22-83PC 60019; Mobil Research and Development Co.: Paulsboro, NJ, 1985.

[17] Kolbel, H.; Ackermann, P.; Ruschenburg, E.; Langheim, R.; Engelhardt,

F. Chem.-Ing.--Tech. **23** (1951) 153.

[18] Wachs, I. E.; Duyer, D. J.; Iglesia, E. Catalysts. Appl. Catal. **12** (1984) 201.

Chapter 5

5.1 General conclusions

Both promoted (Cu, K, Cu/K and SiO_2) and unpromoted $Fe/CaCO_3$ were successfully used to synthesize CNTs using the CVD process. The Cu and K promoted catalysts gave the best yields when compared to the unpromoted and SiO_2 promoted catalysts. The effect of temperature and metal loadings were investigated. When the synthesis temperature was increased from 600 to 700°C the yield of CNTs decreased, when the loading of the promoters were increased from 0.4 to 0.6%, the yield increased and thereafter decreased. The maximum % loading of the promoters used was 1%. Consequently 600°C was chosen as the reaction temperature for CNT synthesis and 0.4 and 0.6% loadings were chosen as optimum loadings of K and Cu respectively.

The CNTs prepared in the presence of the Cu promoted catalyst gave a coiled morphology while the combination of both K and Cu promoters produced a mixture of coiled and straight CNTs. The SiO_2 promoted catalyst also increased the yield of CNTs. The diameters of the promoted catalysts were larger (80 - 100 nm) than those produced from the unpromoted catalyst (60 nm).

The effect of the carrier gas was also investigated. H_2 and N_2 were used as carrier gases. H_2 is known to aid the Fe reduction process, especially at temperatures greater than 500°C and also increase the yield of CNTs. The use of N_2 resulted in lower yields of CNT as less Fe would be in a reduced state and hence the catalytic behaviour was lowered. However the use of H_2 resulted in higher yields of CNTs. The quality of the CNTs produced under N_2 was found to be excellent compared to those produced under H_2.

The materials were successfully characterized by different techniques: TGA, BET surface area, TEM, SEM, EDX and Raman spectroscopy. It was found that the decomposition in air of CNTs purified by diluted HNO_3 acid showed about 98% weight loss for the promoted and unpromoted CNTs. The SiO_2 promoted CNTs were purified by diluted HF and showed only about 75% weight loss due to incomplete extraction of SiO_2 by HF from the CNTs. For CNTs that were

synthesized under N_2, the Cu promoted and unpromoted CNTs lost about 90 and 91% mass respectively, while K containing CNTs lost about 77%.

The surface area of K and SiO_2 promoted catalyst decreased while addition of Cu increased the surface area. TEM and SEM revealed that the morphology and diameters of CNTs mentioned above. All the CNTs were multiwalled in nature with varied size distribution. EDX analysis confirmed the absence and presence of the specific metal. Raman spectroscopy was used to measure the tube quality and it was observed that in general a higher degree of disorder i.e. more defects was detected for promoted Fe catalysts, the exception being Fe-K.

Promotional effects of the Fe/CNT catalyst for FT synthesis were examined and the activity, selectivity, and CO conversions were recorded. K was found to increase the hydrocarbon yield and the CO conversion. The K promoted catalyst increased the CO reaction rate. Addition of K on Fe/CNT also increased the olefinity and the alpha value. The effect of K on the olefinity of the C_2 hydrocarbon is from 0.04 to 0.26. An increase in FTS activity was also observed for the K promoted catalyst. Cu decreased the reduction temperature of ion oxides as noted by TPR studies. The Cu promoted catalyst showed a high selectivity to methane and a decrease of C_{5+}. The C_2 olefins also decreased.

5.2 Future Research

For future work it would be interesting to further examine the role of the Cu, K, and SiO_2 by themselves on carbon nanotube synthesis and see what the differences between these materials and the ones from this study are.